© 2014. Published by The Company of Biologists Ltd | Development (2014) 141, 3483-3494 doi:10.1242/dev.106450

RESEARCH ARTICLE

Histone H3.3 regulates dynamic chromatin states during spermatogenesis

Benjamin T. K. Yuen[1,2,3], Kelly M. Bush[1,2,3], Bonnie L. Barrilleaux[1,2,3], Rebecca Cotterman[1,2,3] and Paul S. Knoepfler[1,2,3,*]

ABSTRACT

The histone variant H3.3 is involved in diverse biological processes, including development, transcriptional memory and transcriptional reprogramming, as well as diseases, including most notably malignant brain tumors. Recently, we developed a knockout mouse model for the *H3f3b* gene, one of two genes encoding H3.3. Here, we show that targeted disruption of *H3f3b* results in a number of phenotypic abnormalities, including a reduction in H3.3 histone levels, leading to male infertility, as well as abnormal sperm and testes morphology. Additionally, null germ cell populations at specific stages in spermatogenesis, in particular spermatocytes and spermatogonia, exhibited increased rates of apoptosis. Disruption of *H3f3b* also altered histone post-translational modifications and gene expression in the testes, with the most prominent changes occurring at genes involved in spermatogenesis. Finally, *H3f3b* null testes also exhibited abnormal germ cell chromatin reorganization and reduced protamine incorporation. Taken together, our studies indicate a major role for H3.3 in spermatogenesis through regulation of chromatin dynamics.

KEY WORDS: Epigenetics, Fertility, Germ cells, Histone variant H3.3, Spermatogenesis, Chromatin, *H3f3b*

INTRODUCTION

During spermatogenesis, a complex interplay of histone post-translational modifications (PTMs) take place in the nuclei of immature germ cells as they develop into mature spermatozoon (Chen et al., 1998; Godmann et al., 2007; Lewis et al., 2003; Payne and Braun, 2006; Rathke et al., 2013; Tachibana et al., 2007; van der Heijden et al., 2006; Zheng et al., 2008). Together with such histone PTMs, histone variants play a major role in the protamine transition and chromatin reorganization process during spermatogenesis, and many histone variants of histone H1 (H1t, H1T2 HILS1), H2A and H2B (TH2A, TH2B, ssH2B, H2A.B.bd, H2BL1, H2BL2, H2AL1-H2AL3) and H3 (H3t, H3.3) become expressed in specific germ cell types or are testes-specific (Lewis et al., 2003; Rathke et al., 2013). The N-terminal tail of H3 acquires specific PTMs during spermatogenesis, including methylation of residue Lys9, a mark involved in chromatin condensation and gene repression, although other residues, such as Lys27 of H3 and Lys20 of H4 also undergo PTM and play roles in establishing repressive chromatin (Jenuwein and Allis, 2001; Kouzarides, 2007; Payne and Braun, 2006). Aberrant regulation of H3 PTMs leads to germ cell apoptosis, defective spermiogenesis and infertility (Iwamori et al., 2011; Liu et al., 2010; Okada et al., 2007; Peters et al., 2001; Tachibana et al., 2007).

Histone variant H3.3 is encoded by two genes in *Mus*, *H3f3a* and *H3f3b*, although both *H3f3a* and *H3f3b* transcripts contain divergent 5′- and 3′-untranslated regions and regulatory sequences that mediate at least partially distinct expression patterns (Akhmanova et al., 1995; Szenker et al., 2011; Witt et al., 1997). H3.3 is incorporated into chromatin in transcriptionally active regions undergoing nucleosome displacement; this is in contrast to the canonical histone H3.1 and H3.2 proteins, which are deposited into chromatin in a replication-dependent manner (Ahmad and Henikoff, 2002; Ray-Gallet et al., 2011; Tagami et al., 2004). This difference is due in part to the unique structure of H3.3, which differs from H3.1 and H3.2 by five and four amino acids, respectively. Of particular importance, H3.3 contains unique Ala87, Ile89 and Gly90 residues, which grant H3.3 the ability to destabilize nucleosomes in transcriptionally active regions (Ahmad and Henikoff, 2002; Jin et al., 2009).

Loss of H3.3 through disruption of either *H3f3a* or *H3f3b* causes defects in fertility (Bush et al., 2013; Couldrey et al., 1999; Hodl and Basler, 2009; Sakai et al., 2009; Tang et al., 2013). H3.3 is expressed throughout the mouse seminiferous tubule (Bramlage et al., 1997) and accumulates in the sex body of spermatocytes (van der Heijden et al., 2007). H3.3 is also not completely removed from chromatin during spermiogenesis (Erkek et al., 2013; Hammoud et al., 2009), and the relatively small remaining H3.3 fraction is enriched in genomic regions important for zygotic development, potentially transmitting a parental epigenetic memory between generations (Erkek et al., 2013; Hammoud et al., 2009). Thus, H3.3 appears to play a crucial role in male spermatogenesis, although the cellular and molecular mechanisms by which H3.3 influences fertility largely remain an open question.

We recently generated an *H3f3b* null mouse model (Bush et al., 2013). Surviving *H3f3b* null males (hereafter referred to as null) displayed complete infertility. Here, we explore the mechanisms involved in the male infertility phenotype. Null male mice have abnormal testes and sperm morphology. Null males also exhibit increased rates of apoptosis in specific germ cell populations and in sperm, and aberrant levels of histone PTM and spermatogenesis-related gene expression within the testes. Finally, null testes display defective germ cell chromatin reorganization and a failure of normal protamine incorporation. These studies overall indicate that H3.3 plays an important role in regulating chromatin states, which are involved in proper male mouse germ cell development.

RESULTS

Loss of *H3f3b* in testes disrupts normal H3.3 deposition during spermatogenesis

To examine the extent of H3.3 histone protein reduction upon homozygous targeted disruption of *H3f3b*, we first examined

[1]Department of Cell Biology and Human Anatomy, Shriners Hospital For Children Northern California, Sacramento, CA 95817, USA. [2]Genome Center, University of California Davis School of Medicine, Shriners Hospital For Children Northern California, Sacramento, CA 95817, USA. [3]Institute of Pediatric Regenerative Medicine, Shriners Hospital For Children Northern California, Sacramento, CA 95817, USA.

*Author for correspondence (knoepfler@ucdavis.edu)

Received 27 November 2013; Accepted 18 July 2014

Development (2014) 141, 3483-3494 doi:10.1242/dev.106450

whole-testes cell lysate (WTCL). Loss of *H3f3b* did not lead to significant changes in total H3 levels in WTCL (supplementary material Fig. S1A,B) but resulted in a >2-fold reduction in H3.3 protein levels (supplementary material Fig. S1C-E, P=0.005), similar to previous reports following *H3f3b* loss in mouse embryonic fibroblasts (MEFs) (Bush et al., 2013). Notably, several faint, but consistently higher molecular-mass H3.3 bands were evident in wild-type (WT) samples but not in those from null mice (supplementary material Fig. S1C,D), indicating the involvement of larger, uncharacterized H3.3-specific PTMs in testes, because these PTMs were not observed in other cell types.

H3f3a transcripts are expressed throughout the testes (spermatogonia, spermatocytes and spermatids) at low levels, whereas *H3f3b* is most highly expressed specifically in spermatocytes (Bramlage et al., 1997). We utilized an H3.3-specific antibody for immunohistochemistry-based immunofluorescence staining (IHC-IF) in mouse testes sections from *H3f3b* WT and null male animals, along with a lectin peanut agglutinin (lectinPNA) conjugate that recognizes the sperm acrosome used to stage-match testes cross-sections (Aviles et al., 1997; Szasz et al., 2000). H3.3 protein accumulated in the nuclei of spermatogonia and leptotene spermatocytes (Fig. 1A,B) in WT tubules. Nuclear H3.3 levels peaked during mid-stage in WT pachytene spermatocytes and persisted throughout meiosis and most of spermiogenesis, with H3.3^{+} focal regions appearing within the nuclear interior of WT pachytene and diplotene spermatocytes (Fig. 1A,C; supplementary material Fig. S1F, G), corresponding to regions resembling the sex body (van der Heijden et al., 2007). WT step 1-8 round spermatids expressed H3.3 throughout the nucleus and at bright focal points within the nuclear interior, most likely to be the sex body described previously in *Mus* (van der Heijden et al., 2007) (supplementary material Fig. S1F,G). Relative H3.3 levels began to decrease in step 11 WT elongating spermatids (Fig. 1C) and were undetectable in step 12-16 spermatids (supplementary material Fig. S1F,G).

As expected, null tubules displayed substantially lower levels of H3.3 by IHC-IF analyses. H3.3 was nearly undetectable in spermatogonia, pre-leptotene, leptotene, zygotene and early pachytene (stage I-II) spermatocytes in null tubules. Faint nuclear expression of H3.3 became apparent in mid-stage (stage IV-V) null spermatogonia (supplementary material Fig. S1F) as opposed to those of WT, in which H3.3 expression was first detected in early spermatogonia populations. Weak nuclear focal expression of H3.3 was seen in early- to mid-stage null pachytene spermatocytes (stage III-V, supplementary material Fig. S1F,G), but the diffuse nuclear staining was never comparable in intensity to that observed in WT. Nuclear and focal areas of H3.3 protein localization in step 1-11 spermatids were also substantially fainter in null testes, and H3.3 was undetectable by IHC-IF in step 12-16 spermatids. Thus, knockout of *H3f3b* results in substantial decreases in H3.3 protein levels throughout spermatogenesis in a number of cell types within the seminiferous tubule (supplementary material Fig. S2), with the remaining low levels of H3.3 produced from *H3f3a*.

Loss of *H3f3b* leads to male testes atrophy and decreased germ cell types

We examined WT and surviving null mature male mice (supplementary material Fig. S3 and Table S1 for age ranges, P=0.420) for defects. Nulls possessed smaller testes, both when compared with their WT littermates and when normalized to animal mass (supplementary material Fig. S3A-E). Compared with WT testes histological sections (supplementary material Fig. S3F), null seminiferous tubules exhibited abnormal architecture, with small and unusually open tubules and reduced numbers of germ cell types and early spermatozoa.

To determine the effect of *H3f3b* loss on spermatid quantity within a tubule cross-section, we measured the number of stage I round (step 1) and elongated (step 13) spermatids in WT and null tubules. Step 1 round spermatids are the direct result of meiotic divisions in spermatocytes that take place in the preceding stage XII tubules. We observed a significant 1.46-fold decrease in the total number of

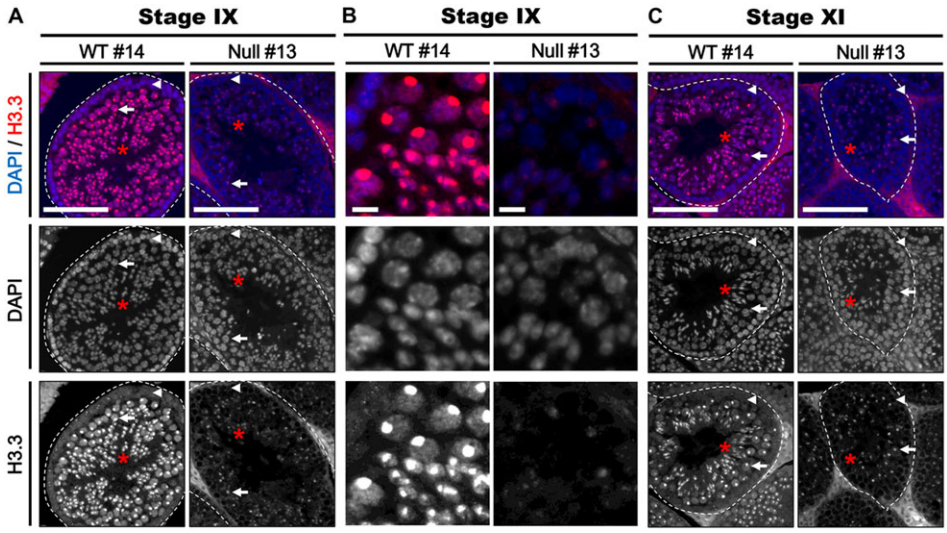

Fig. 1. Alterations of the normal levels and patterns of H3.3 protein in *H3f3b* null testes. Immunohistochemistry staining of WT and null testes sections. (A) H3.3 (red) protein is present in WT stage IX tubules in spermatogonia and leptotene spermatocytes (white arrowhead), in pachytene spermatocytes (white arrow) and in elongating spermatids (red star). Null tubules show little or no H3.3 staining in spermatogonia and leptotene spermatocytes at this stage, and H3.3 is only weakly evident in pachytene and elongating spermatids. (B) Higher magnification images more clearly show considerable reductions in H3.3 staining in null stage IX spermatocytes and elongating spermatids. (C) H3.3 is strongly expressed in WT diplotene spermatocytes (white arrow) and weakly in elongated spermatids (red star) and in zygotene spermatocytes (white arrowhead). Null tubules exhibit weak focal H3.3 protein in diplotene spermatocytes and elongated spermatids, with no nuclear H3.3 staining. H3.3 was nearly undetectable in zygotene spermatocytes in null tubules. DAPI (blue) was used for counterstaining. Scale bars 100 µm (A,C); 10 µm (B). White dotted lines indicate borders of specified tubule. Staining was performed using n=2 WT and n=4 null animals.

Development (2014) 141, 3483-3494 doi:10.1242/dev.106450

spermatids per null tubule area (supplementary material Fig. S3G), comprising a 1.36-fold decrease in round spermatids and a 1.6-fold decrease in elongated spermatids at this stage (supplementary material Fig. S3H,I). In order to further investigate potential changes in germ cell quantity, we used fluorescence-activated cell sorting (FACS) based on previously established protocols (Bastos et al., 2005; Gaysinskaya et al., 2014; Getun et al., 2011) on testes from two WT and four null aged males (see supplementary material Table S1). We utilized FACS to successfully separate spermatogonia, pre-leptotene spermatocytes, spermatocytes and spermatids with a high degree of enrichment (supplementary material Fig. S4A-H). The FACS profiles of WT and null populations showed high similarity in cell type distribution, although null testes contained substantially fewer cells overall (supplementary material Fig. S5A,B). Null testes exhibited comparable populations of spermatogonia and spermatocytes (supplementary material Fig. S5C,D) and a slight but significant increase in spermatid number (supplementary material Fig. S5E, P=0.033). These data suggest that despite the observed decrease in spermatid numbers per tubule cross-section, the overall proportion of spermatids in relation to other germ cell types is similar to that of WT. Null testes also exhibited a 1.9-fold decrease in the number of pre-leptotene spermatocytes (supplementary material Fig. S5F, P=0.020), indicating increased cell death in this population, or fewer spermatogonia transitioning into this cell type.

Loss of *H3f3b* has been reported to cause defects in chromosome segregation (Bush et al., 2013). We quantified the number of stage XII meiotic tubules in WT and null testes to determine whether *H3f3b* loss leads to a higher preponderance of stalled meiotic tubules by utilizing immunostaining of phosphorylated residue Ser10 on H3 (H3 S10P), a marker of mitotic and meiotic cells (Korhonen et al., 2011). Null testes exhibited a slight, but non-significant, increase in the proportion of meiotic tubules per absolute number of seminiferous tubules (12.3%) compared with WT (10.7%) (supplementary material Fig. S6A). We did not detect a difference in the number of meiotically dividing cells within a tubule when normalized to the tubule area (supplementary material Fig. S6B, P=0.923). Removal of *H3f3b* was previously shown to affect Cenpa incorporation and possibly contribute to centromere dysfunction in MEFs (Bush et al., 2013). We did not observe an increase in the number of Cenpa^{+} foci per spermatogonia or spermatocyte in null tubules (supplementary material Fig. S6C,D). These findings suggest that the observed changes in spermatid populations are not likely to result from defective meiotic processes.

H3f3b null males exhibit reduced sperm concentration, abnormal sperm morphology and apoptotic events in spermatocyte and spermatogonia cell types

To further explore the mechanisms of *H3f3b* null male infertility, we analyzed the sperm of WT-control and null males (Table 1). Null males exhibited >2-fold decrease in total sperm concentration. The null sperm that were present were quite abnormal, exhibiting >2-fold decreases in motility, >3-fold decreases in rapid cells and >4-fold decreases in progressive motility (supplementary material Movies S1, S2). Examination of WT and null sperm under high magnification revealed major abnormalities in morphology (Fig. 2A), with 99% of null sperm having abnormal heads (versus 30% of WT), indicating possible defects in meiotic chromatin condensation (Fig. 2B).

We also examined the potential effects that *H3f3b* loss would have on cell survival in the testes. We observed a 2.06-fold increase in the percentage of apoptotic tubules per null testis (Fig. 2C, classified as exhibiting one or more TUNEL^{+} nuclei per tubule) and a 1.63-fold increase in the absolute number of apoptotic tubules per null testis relative to WT (Fig. 2D). Null tubules also exhibited a significant 3.53-fold increase in apoptotic events (4.25% of null cells versus 1.20% of WT) (Fig. 2E). In null testes, the majority of apoptotic events took place in or around stage IX tubules, within one to two cell-layers from the tunica propria, where pre-leptotene spermatocytes transition into leptotene spermatocytes (Fig. 2F; supplementary material Fig. S2, Fig. S7A,D), with few apoptotic nuclei detected in early (stage I-V) and nearly no apoptotic nuclei detected during mid-stage (stage VI-VIII). Null tubules also exhibited very high levels of TUNEL^{+} nuclear fragments, which were essentially absent in the WT tubules (Fig. 2F, red stars). Examination of subsequent stages corroborated these findings because stage X tubules also contained increased numbers of apoptotic nuclei one to two cell-layers away from the tunica propria, corresponding to leptotene and pachytene spermatocytes (supplementary material Fig. S7B). Often, TUNEL^{+} null tubule sections in the stages following stage IX exhibited small and degraded apoptotic nuclei near the tunica propria, suggesting that these nuclear fragments are the remnants of earlier apoptotic nuclei (supplementary material Fig. S7B,C).

Table 1. Summary of sperm characteristics in *H3f3b* null mice

Genotype	Concentration (M/ml)	Motile (%)	Progressive movement (%)	Rapid cells (%)
H3f3b WT*	37.00±5.71	72.67±11.86	40.67±10.73	60.33±13.78
H3f3b null*	15.48±2.70	27.00±8.68	9.60±3.41	17.60±5.71
t-test‡	7.96×10^{-3}	0.020	0.014	0.015
Reference	20-50	>40	>15	>30

Summary of sperm characteristics in *H3f3b* null males. Null males exhibit significantly reduced sperm concentration as well as a reduced percentage of motile sperm, sperm capable of progressive movement and sperm capable of rapid movement. Reference ranges are from UCD Mouse Biology Program.
*Mean±s.e.m.
‡Student's two-tailed *t*-test.
Sperm measurements were taken from n=3 WT and n=5 null animals.

H3f3b deficiency results in sharply elevated H3K9me3 levels in distinct germ cell populations

Because histone PTM plays key roles in spermatogenesis, we sought to determine whether aberrant histone methylation could play a role in the observed defects in *H3f3b* null testes. We utilized IHC-IF to examine the levels of H3 Lys9 trimethylation (H3K9me3), a mark associated with transcriptional silencing and heterochromatin. H3K9me3 levels were strikingly higher overall in null testes when compared with those of WT (supplementary material Fig. S2, Fig. S8A). WT mice exhibited patterns of H3K9me3 staining that were consistent with previous reports of H3K9me3 in normal mouse testes, in which H3K9me3 was found in spermatogonia, pre-leptotene, leptotene and pachytene spermatocytes, and in the chromocenters of round spermatids (Iwamori et al., 2011; Liu et al., 2010; Payne and Braun, 2006). By contrast, in nulls, nuclear H3K9me3 staining was relatively more intense in spermatogonia, pre-leptotene, leptotene, zygotene and early (stage I-V) pachytene spermatocytes (supplementary material Fig. S9, Fig. S10). H3K9me3 levels did gradually decrease from pachytene to diplotene stages of meiotic prophase (Fig. 3A,B), although H3K9me3 levels were still higher in null tubules. H3K9me3 nuclear foci with intensities much higher than those seen in WT persisted in null pachytene spermatocytes and step 1-13 spermatid chromocenters, and null tubules typically exhibited more brightly stained focal points in secondary or meiotic spermatocytes when compared with WT (Fig. 3C).

Development (2014) 141, 3483-3494 doi:10.1242/dev.106450

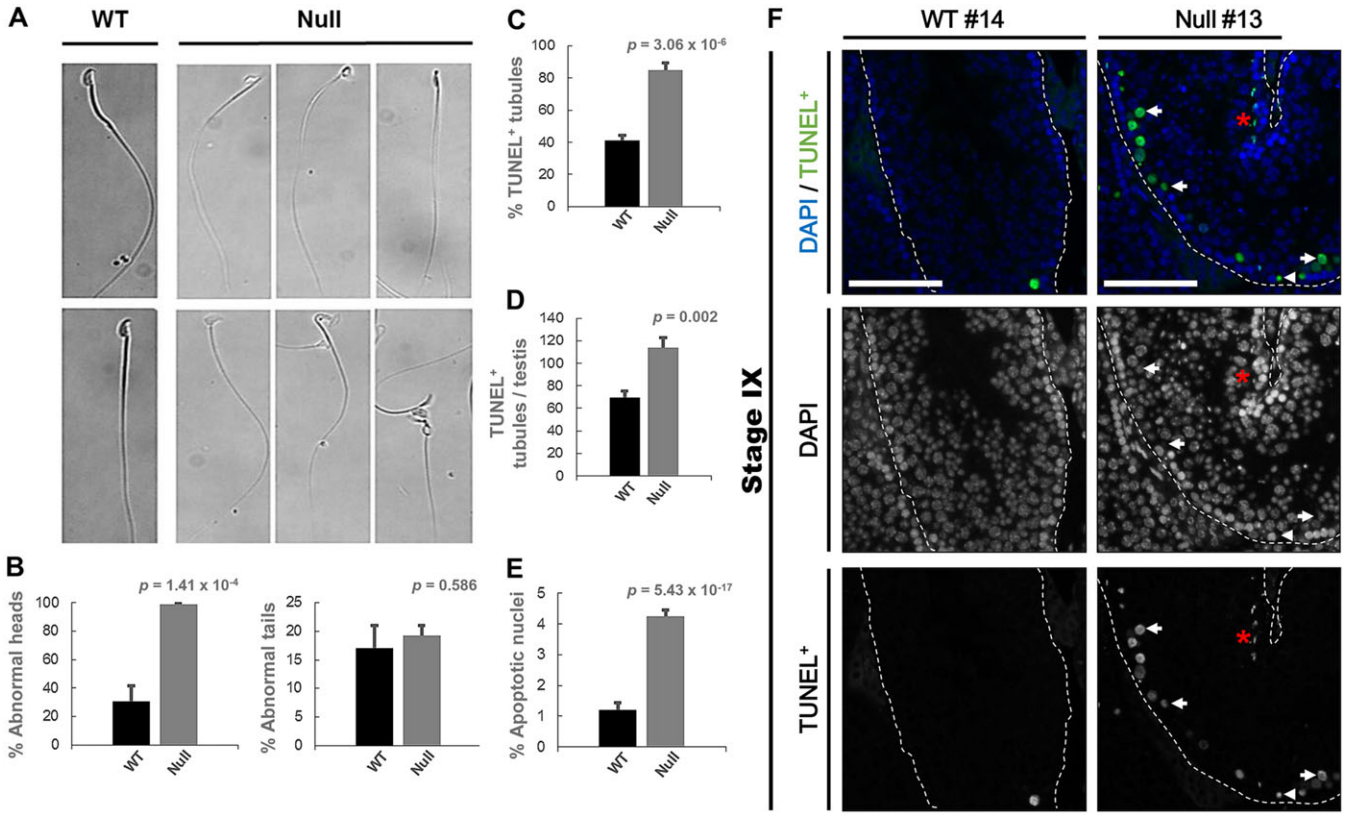

Fig. 2. Gross defects in null sperm and increased germ cell apoptosis upon targeted disruption of *H3f3b*. (A) Sperm from *H3f3b* null animals display abnormal characteristics compared with their WT counterparts. A variety of defects found in null sperm are shown in these representative images. (B) Analysis of sperm. Data presented are means±s.e.m. (C,D) Null testes exhibit a significant 2.06-fold increase in the percentage of apoptotic tubules per testis (C) and a significant 1.63-fold increase in the absolute number of apoptotic tubules per testis (D). (E) Nulls exhibited a 3.5-fold increase in the percent of apoptotic nuclei per tubule. (F) Apoptotic events were primarily detected one to two cell-layers luminally from the tunica propria of the seminiferous tubule. White arrowheads indicate spermatogonia, white arrows indicate leptotene and/or pachytene spermatocytes and red stars indicate regions containing fragmented apoptotic nuclei. DAPI (blue) was used for counterstaining. Scale bars: 100 µm. White dotted lines indicate borders of specified tubule. Sperm measurements were taken from *n*=3 WT and *n*=5 null animals. TUNEL staining was performed on *n*=4 WT and *n*=6 null animals.

When we enriched for histone-containing chromatin proteins using acid extraction on whole testes, we observed a 1.85-fold increase in the levels of H3K9me3 relative to those of total H3 by immunoblotting samples from null males (P=0.001, Fig. 3D,E). By contrast, the amount of H3K9me3 relative to β-actin in WTCL from nulls was not elevated (P=0.287, supplementary material Fig. S8B-D). To determine whether H3K9me3 accumulates specifically in the cell types in which we observed TUNEL$^+$ events, we stained pre-leptotene spermatocytes and spermatocytes for H3K9me3. Sorted pre-leptotene spermatocytes exhibited a 1.97-fold higher level of H3K9me3, through IHC-IF analyses, relative to WT (supplementary material Fig. S8E,F, P<0.001). Sorted null spermatocytes and null γH2A.X$^+$ spermatocytes (primarily pachytene cells) generally displayed higher levels of H3K9me3, although this difference was not significant (supplementary material Fig. S8G,H).

To determine whether *H3f3b* loss could affect other PTMs, we also examined levels of the euchromatic Lys4 trimethylation mark on H3 (H3K4me3) and the repressive Lys27 trimethylation mark on H3 (H3K27me3) in WT and null testes. We were able to detect a small, yet consistent decrease in the levels of H3K4me3 in null testes by IHC-IF (supplementary material Fig. S11A) but were unable to discern a difference in specific localization patterns between WT and null tubules. H3K4me3 levels were slightly decreased in null WTCL when compared with that from WT littermates, although overall this decrease was not significant (supplementary material Fig. S11B,C). H3.3 is enriched for euchromatic marks, such as H3K4me3 (Hake et al., 2006; McKittrick et al., 2004), and the observed decreases could reflect a loss of H3K4me3-bearing H3.3 histones. We were also unable to detect a significant difference in the amount of H3K27me3 between the two genotypes through analyses of WTCL (supplementary material Fig. S11D) or IHC-IF analyses (data not shown). We observed significant increases in the relative phosphorylation levels of the H3.3-specific Ser31 residue (H3.3 S31P) in null testes (supplementary material Fig. S11D, compared with the total H3.3 protein levels in the same samples shown in supplementary material Fig. S1C-E), suggesting that the remaining H3.3 protein in nulls might become hyper-phosphorylated on Ser31, as described previously (Bush et al., 2013). Notably, H3.3 S31P was found to localize primarily to meiotically dividing spermatocytes in stage XII tubules (supplementary material Fig. S11E) in samples from both WT and null mice. These results suggest that loss of H3.3 primarily affects H3K9me3 PTM at specific timepoints in spermatogenesis, particularly during the pre-leptotene to leptotene transition.

H3f3b loss disrupts the expression of crucial spermatogenesis-related genes

We isolated RNA from *H3f3b* WT and null testes and conducted gene expression microarray studies. Employing a 2-fold or greater expression change cutoff, only six genes were up- or downregulated

Development (2014) 141, 3483-3494 doi:10.1242/dev.106450

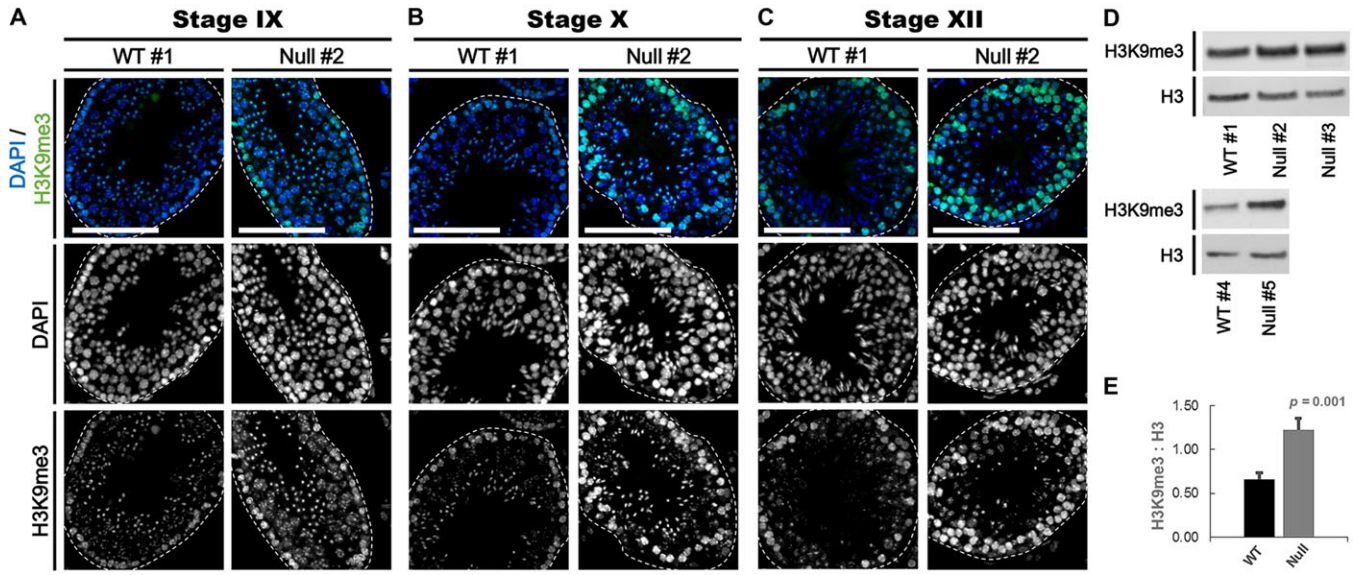

Fig. 3. Histone H3.3 influences H3K9me3 levels in late-stage tubules. Immunohistochemistry staining for H3K9me3. (A) The H3K9me3 (green) signal was strongest in null spermatogonia, leptotene spermatocytes and focal points in elongating spermatids, and was diffuse in pachytene spermatocytes. (B) The H3K9me3 levels in stage X tubules were strongest in null spermatogonia and leptotene spermatocytes, but were weaker along the tubule lumen in pachytene spermatocytes and elongating spermatids. (D) H3K9me3 staining was strongest in spermatogonia and zygotene spermatocytes, with weak focal staining of meiotic spermatocytes and spermatids in stage XII null tubules. (D) Null males demonstrated increased H3K9me3 levels relative to the total H3 levels in nuclear acid extracts. (E) Nulls exhibit a 1.85-fold increase in the H3K9me3:H3 ratio (P=0.001). DAPI (blue) was used for counterstaining. Scale bars: 100 µm. White dotted lines indicate borders of specified tubule. H3K9me3 staining was performed on n=4 WT and n=6 null animals.

by loss of *H3f3b,* with one of the downregulated genes being *H3f3b* itself (supplementary material Table S2). Using a 1.5-fold cutoff, 186 and 375 genes in total were up- and downregulated in testes by loss of *H3f3b*, respectively (supplementary material Table S3). Importantly, the expression changes in 45 of the up- and 111 of the downregulated genes were shared events in both samples from null mice (supplementary material Table S3). Database for annotation, visualization and integrated discovery (DAVID) gene ontology (GO) analysis (Huang et al., 2009a,b) revealed that the most prominent ontological cluster of genes downregulated using the 1.5-fold cutoff were genes associated with sperm and spermatogenesis. These genes included *Catsper1* and *Catsper3* (cation channel, sperm associated 1 and 3), *Spaca3* and *Spaca4* (sperm acrosome 3 and 4), the flagellum associated gene *Cabyr*, the spermatozoa associated *Hook1* and the spermatogenesis-linked adipogenin (*Adig*) related cDNA (*BC054059*). Validation quantitative (q) PCR measurements of *Catsper1*, *Spaca3*, *Adig/BC054059* and *Hook1* levels confirmed that these fertility-linked genes were significantly decreased in null adult testis relative to that of WT littermates (Fig. 4A). GO analysis of expression data also indicated that genes found to be upregulated in the null testes were ontologically enriched for an ‘induction of apoptosis’ functional cluster. Downregulated genes tended to be localized away from CpG-rich regions, whereas 61% of upregulated genes trended the opposite way (supplementary material Table S4). Deregulated genes were not enriched on any particular chromosome (supplementary material Table S4).

For a more detailed analysis invoking a cell-type specific component, we utilized mouse transcriptome data from the Gene Expression Omnibus (GEO) database (GSE21749, GSE4193, GSE23119 and GSE21447) to determine the expression pattern of *H3f3b* null up- and downregulated genes in normal, staged germ cell populations, as performed previously (Gaucher et al., 2012; Tan et al., 2011). Importantly, the majority of genes found to be downregulated by 1.5-fold or more in null testes are normally, and predominantly, expressed in round spermatids and moderately in spermatogonia (Fig. 4B). This pattern is logical given that a large proportion of downregulated genes was enriched for functional processes involving sperm development. By contrast, the majority of genes upregulated by 1.5-fold or greater are normally expressed in spermatogonia and early spermatocyte (pre-leptotene, leptotene, zygotene) populations (Fig. 4C), the same populations of cells that exhibited an increase in apoptotic events upon TUNEL staining, although it is important to note that pre-leptotene spermatocytes were found to be significantly decreased through FACS analysis in the null.

ChIP-seq analysis reveals epigenomic changes in *H3f3b* nulls

We performed ChIP-seq for H3K4me3 in WT and null testes samples (two biological replicates each). Globally, loss of reads mapping to the *H3f3b* locus was apparent in both null samples, validating the null genotype (supplementary material Fig. S12A). Both null samples had fewer H3K4me3 peaks than both WT samples, and the peaks were on average narrower in null samples than those of WT (supplementary material Table S5). We constructed consensus peak sets for WT and null samples by intersecting the peaks of each replicate. The WT consensus peak set contained 27% more H3K4me3 peaks than the null consensus peak set (Fig. 4D), and the WT peaks were an average of 39% broader than the peaks of the null samples (1680 versus 1210 bp, P<0.0001, supplementary material Fig. S12B). Nearly all of the peaks in the null samples were also found in the WT samples (97%), whereas 23% of the WT consensus peaks were absent from the null consensus peak set. The two WT samples were very similar to each other, with ~90% overlapping peaks (supplementary material Fig. S12C). However, null samples were more divergent; only 81% of the peaks from null sample 73 were also found in null sample 67 (supplementary material Fig. S12D). We used the R package ‘DiffBind’ to cluster the ChIP-seq data and determine the correlation between samples. WT samples were highly similar to each other (correlation>0.94), whereas the null samples, although

Development (2014) 141, 3483-3494 doi:10.1242/dev.106450

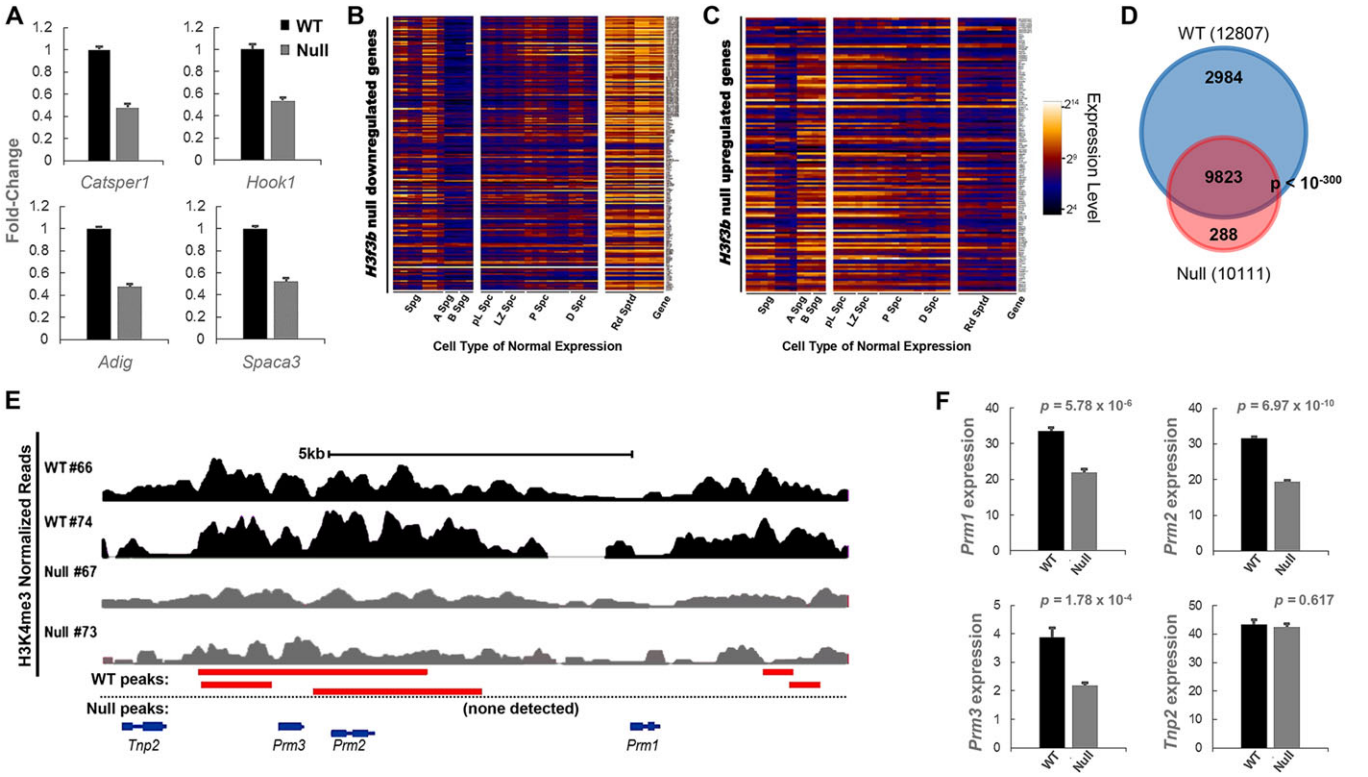

Fig. 4. The influence of H3.3 on transcriptional processes and H3K4me3 within the testes. (A) qPCR analysis for fertility related genes *Catsper1*, *Spaca3*, *Adig*/*BC054059* and *Hook1*. Error bars indicate s.d. (B) Genes downregulated, upon array analysis, in null testes are normally expressed in round spermatids, with moderate expression in spermatogonia. Spermatogonia (Spg), A-type Spg (A Spg), B-type Spg (B Spg), pre-leptotene spermatocyte (pL Spc), leptotene/zygotene spermatocyte (LZ Spc), pachytene spermatocyte (P Spc), diplotene spermatocyte (D Spc) and round spermatids (Rd Sptd) array sample columns are shown. (C) Upregulated null genes are expressed normally in spermatogonia and early spermatocyte populations. (D) WT and null samples exhibit a high degree of consensus H3K4me3 peak set overlap using ChIP-Seq analysis. Numbers in parentheses indicate the total number of peaks in each cell type. (E) Compared with WT (black), null (gray) testes display reduced H3K4me3 ChIP-seq peaks around the protamine domain, with a specific loss of peaks around *Prm1-Prm3* and *Tnp2*. Peaks called by HOMER are shown as red bars below. (F) qPCR analyses of whole testes RNA reveals significant decreases in *Prm1-Prm3*, but not *Tnp2* expression in *H3f3b* nulls.

similar in an absolute sense, were relatively less alike to each other (correlation<0.90). The two null replicate samples specifically clustered together, as did the two WT samples with each other, demonstrating that loss of *H3f3b* might result in both overlapping, but also distinct gene expression changes (supplementary material Fig. S13A). DiffBind identified 281 peaks that were significantly reduced in null samples, and 90 peaks that were significantly increased in null samples compared with those of WT (supplementary material Table S6). No consistent pattern of changes in the frequency of satellite repeats were observed in the nulls (supplementary material Fig. S13B).

H3K4me3 peaks increased in null were enriched for embryonic development genes, whereas the decreased peaks were enriched for spermatogenesis genes (supplementary material Tables S6, S7). We found a significant overlap between differentially regulated genes in the nulls that were identified by microarray analyses and genes exhibiting unique or increased and/or decreased patterns of H3K4me3 through ChIP-seq analyses in the nulls (supplementary material Fig. S14A-D). qPCR analyses of overlapping genes between the microarray and H3K4me3 ChIP-seq datasets verified that changes in transcription were reflected in the upregulation or gain of H3K4me3 peaks (supplementary material Fig. S13C-E) or the downregulation or loss of peaks (supplementary material Fig. S13F-H). Notably, both null samples exhibited a loss of H3K4me3 peaks around the protamine domain cluster, comprising protamine genes 1, 2 and 3 (*Prm1-Prm3*) and transition protein gene 2 (*Tnp2*) (Martins and Krawetz, 2007) (Fig. 4E), and around the transition protein 1 gene (*Tnp1*) (supplementary material Fig. S15A). qPCR analyses on RNA from whole testes revealed significant decreases in *Prm1-Prm3* expression in nulls (Fig. 4F) but surprisingly not in *Tnp1* and *Tnp2* expression (Fig. 4F; supplementary material Fig. S15B), although these results might be affected by differences in germ cell content.

To further explore a loss of expression from the protamine domain cluster in nulls, we examined WT and null spermatids, which had been sorted using FACS. Combined null samples exhibited lower levels of *Prm1* and *Prm2* when compared with combined WT samples (supplementary material Fig. S15C,D), although these differences were not statistically significant. This might be due, in part, to the presence of one outlier null male that exhibited aberrantly high levels of these transcripts (supplementary material Fig. S15E,F). All null males expressed lower levels of *Prm3* (P=0.030) and *Tnp2* (P<0.001) (supplementary material Fig. S15G,H). Null males did not differ from WT in *Tnp1* expression (supplementary material Fig. S15I). Taken together, these data suggest that H3.3 is necessary for the appropriate expression of spermatogenesis-related genes.

H3f3b knockout leads to asynchronous spermatid development during spermiogenesis

We stained testes sections with lectinPNA to follow acrosome development and spermiogenesis in *H3f3b* WT and null tubules.

Development (2014) 141, 3483-3494 doi:10.1242/dev.106450

Null and WT seminiferous tubules were capable of producing acrosomal granules and an acrosomal cap. However, during spermiogenesis, late-stage null tubules displayed asynchronous spermatid elongation. As the abnormal, mixed nature of late-stage null tubules made it difficult to distinguish stage IX tubules from stage X tubules, we classified stage IX as tubules in which the majority of the spermatids were step 9, whereas those at stage X were characterized as containing a majority of step 10 spermatids among a mixture of step 9-11 spermatids in the tubule lumen. Individual sections of late-stage null tubules frequently exhibited spermatids characteristic of a number of different stages.

Stage IX null tubules consistently exhibited aberrant mixed characteristics of (1) late stage VIII tubules, in which spermatozoa have exited the tubule lumen during spermiation and round spermatids persist, and (2) stage X tubules, in which early elongating spermatids begin to become bilaterally flattened (Fig. 5A). Similarly, stage X null tubules, normally containing bilateral flattening spermatids, frequently exhibited characteristics of stage IX and late-stage tubules (e.g. stage XI) (Fig. 5B), a phenotype that was only very rarely present in WT testes. These data suggest that null tubules do not exhibit synchronized chromatin reorganization, which is normally observed during spermiogenesis. It is also possible that this asynchronous development could lead to elevated spermatid numbers during certain stages of spermatogenesis due to delayed spermiation.

H3f3b is required for the switch from histone- to protamine-based chromatin

Tnp1 plays a key role in the transition to protamine-based chromatin that is essential for normal spermatogenesis and fertility (Balhorn, 2007; Braun, 2001; Carrell et al., 2007; Miller et al., 2010; Okada et al., 2007). Tnp1 first becomes strongly expressed in step 11 spermatids (Zhao et al., 2004) and persists until step 13-15 (Yu et al., 2000; Zhao et al., 2004). Null late-stage tubules contained step 8-9 spermatids ($Tnp1^{-}$) and step 10-11 spermatids ($Tnp1^{+}$) within the same tubule, an exceedingly rare occurrence in stage-matched WT tubules (supplementary material Fig. S2; Fig. 5C). In addition, $Tnp1^{+}$ spermatids were abnormally present in a small number of mid-stage null tubules.

To further examine whether *H3f3b* loss affected chromatin reorganization and proper sperm function by interfering with protamine replacement into chromatin, we stained WT and null testes for Prm1. The highest amount of Prm1 protein staining in WT tubules was found in step 11-16 spermatids (stage XI-VIII tubules) (supplementary material Fig. S2; Fig. 6A,B), as previously reported (Zhao et al., 2004). By contrast, Prm1 staining in step 11-16 null spermatids was dramatically reduced (Fig. 6A,B and supplementary material Fig. S16A,B), perhaps a result of, at least in part, the decrease in total spermatids per tubule area and reduced *Prm1* expression. Levels of Prm1 in null tubules was also very weak or undetectable in late, mixed-stage tubules with delayed step 8-9 spermatids present within the luminal area.

Prm1 levels were also decreased in null decondensed sperm (Fig. 6C). Decondensed null sperm also exhibited higher overall levels of H3K9me3 than those of WT (Fig. 6C; supplementary material Fig. S16C) and in a significantly higher proportion of sperm (supplementary material Fig. S16D, $P<0.001$). Null sperm were also found to have a high number of apoptotic nuclei by TUNEL staining (supplementary material Fig. S16C) with 23% of null sperm being $TUNEL^{+}$, 12.1-fold higher than WT ($P<0.001$, supplementary material Fig. S16E). Increased levels of H3K9me3 in null sperm were moderately correlated to the increase in sperm

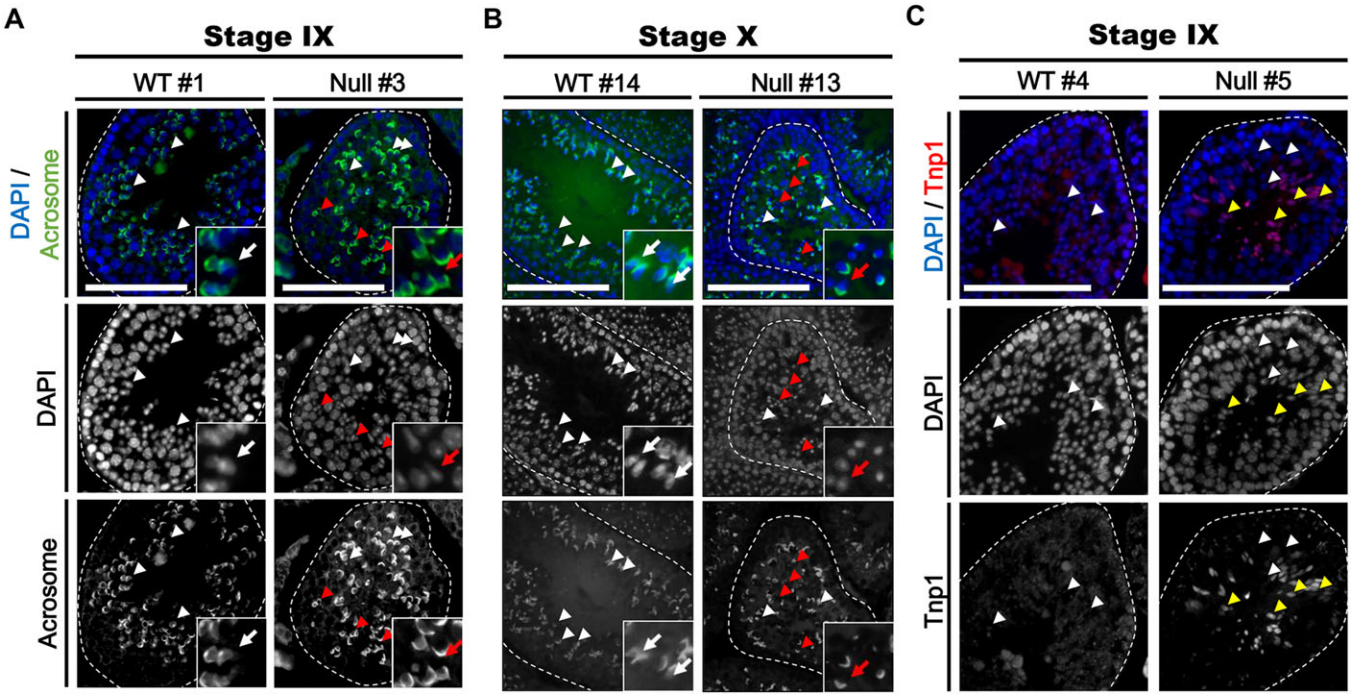

Fig. 5. Knockout of *H3f3b* causes asynchronous chromatin reorganization. (A) Acrosomal (green) staining indicates that WT stage IX tubules typically exhibit a homogenous, normal population of spermatids beginning elongation (white arrows), whereas null tubules display a mixture of spermatid development (red and white arrows). (B) Stage X WT tubules exhibit bilaterally flattening spermatids (white arrows), whereas null tubules frequently display a mixture of elongating or fully elongated spermatids (red and white arrows). Inset images show magnified areas. (C) WT stage IX tubules do not typically display Tnp1 (red) expression (white arrows); by contrast, null tubules present step 9 ($Tnp1^{-}$, white arrows) or later ($Tnp1^{+}$, yellow arrows) in the same tubule. DAPI (blue) was used for counterstaining. Scale bars: 100 µm. White dotted lines indicate borders of specified tubule. Tnp1 staining was performed on $n=4$ WT and $n=5$ null animals.

Development (2014) 141, 3483-3494 doi:10.1242/dev.106450

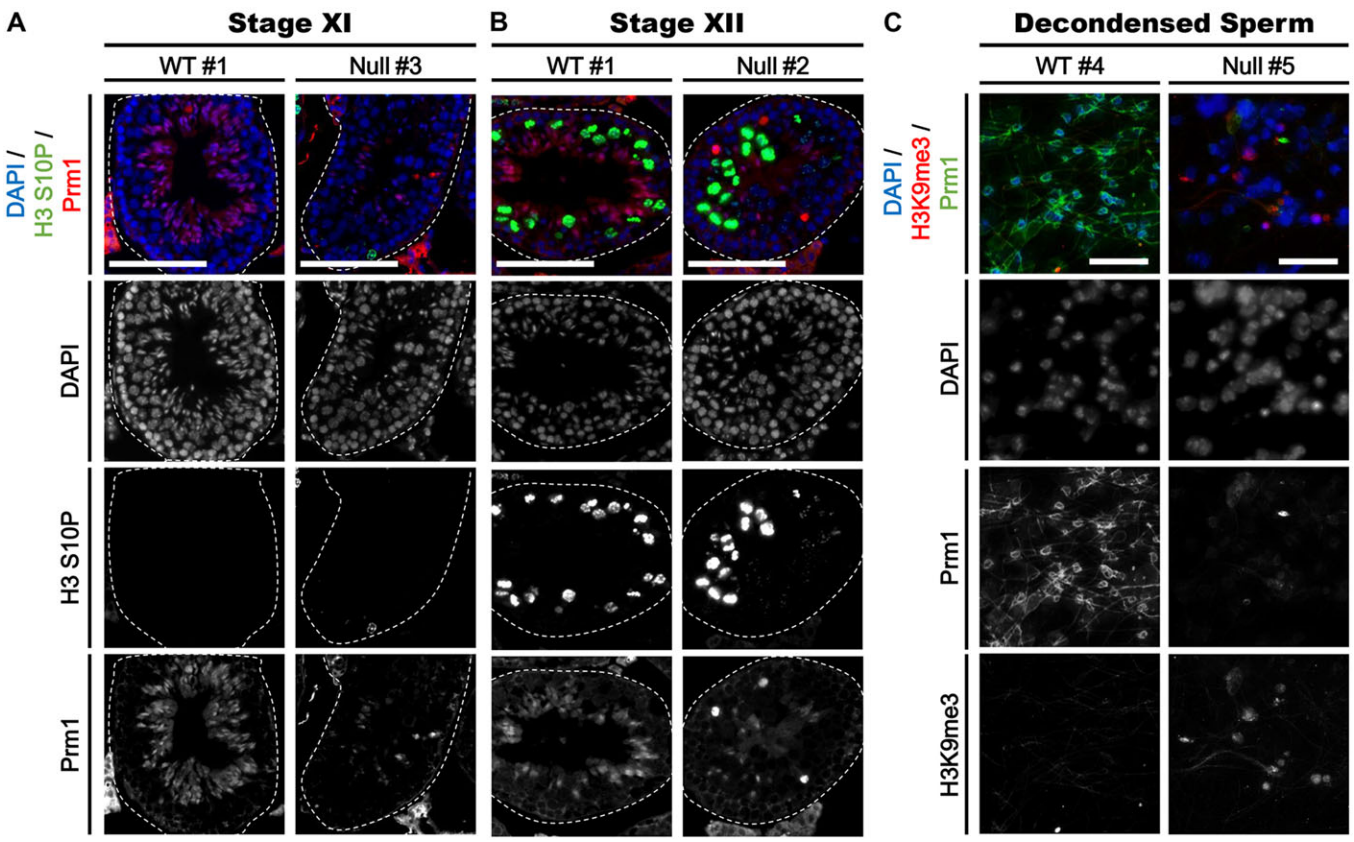

Fig. 6. *H3f3b* is required for appropriate protamine incorporation. (A,B). Immunostaining reveals that Prm1 (red) levels are substantially reduced in null step 11 (A) and step 12 (B) spermatids. H3 S10P (green) staining was used to identify meiotic tubules. (C) Immunostaining of decondensed null sperm demonstrates decreased Prm1 (green) expression and an increase in H3K9me3 (red) expression. DAPI (blue) was used for counterstaining. Scale bars: 100 µm (A,B); 20 µm (C). White dotted lines indicate borders of specified tubule. H3 S10P staining was performed on *n*=2 WT and *n*=3 null animals. Prm1 staining was performed on *n*=3 WT and *n*=4 null animals.

apoptosis, as 18.8% of H3K9me3^{+} sperm were also TUNEL^{+} (P<0.001, supplementary material Fig. S16F). Taken together, these data indicate that H3.3 is necessary for the switch to protamine-based chromatin and for normal chromatin restructuring during spermatogenesis.

DISCUSSION

Here, we found that reduced H3.3 levels, as a result of *H3f3b* knockout, disrupted male reproductive function through developmental defects, resulting in dysfunctional spermatozoa and reduced total spermatozoa numbers. One possible explanation for the decreased sperm concentration could be defects arising in meiosis, although we were unable to discern significant differences in the number of stage XII meiotic tubules or in the number of meiotically dividing spermatocytes in WT and null testes. However, the null cells with the strongest meiotic defects could well be those most prone to apoptosis and hence be lost for analysis. Another explanation is that reduced sperm levels could be due to elevated levels of apoptosis that are not directly related to meiosis; indeed, a substantial proportion of null epididymal sperm exhibited apoptotic nuclei, suggesting that lethal defects arise as a result of earlier events in the generation of the sperm that are disrupted in the null.

Notably, the majority of apoptotic events in null testes occurred in or around stage IX (supplementary material Fig. S2), a period where spermatogonia stem cells differentiating into spermatocytes cross the tightly regulated blood-testis barrier (BTB) (Bordlein et al., 2011; Cheng and Mruk, 2012; Morales et al., 2007; Mruk and Cheng, 2004; Oishi et al., 2004). Downregulated genes in null testes are expressed normally in spermatogonia, a cell type that in null mice also displayed increases in H3K9me3, indicating that an aberrant repressive chromatin state established in the early stages of null spermatogonia development might impede the expression of genes necessary for differentiation into pre-leptotene spermatocytes and the BTB transition.

Strong decreases in H3.3 and increases in H3K9me3 were observed in late-stage null tubules (supplementary material Fig. S2), particularly in spermatogonia and spermatocytes. Western blotting for chromatin-bound H3K9me3 from acid extract revealed a significant increase in levels compared with those of WT. Although this change was not detectable in WTCLs, this discrepancy might be due to the variation in germ cell size within the testes, demonstrated by the fact that the increase of H3K9me3 varied amongst distinct cell types, or because WTCLs include concentrations of non-chromatin bound histones that probably have distinct PTM patterns. A previous study (Okada et al., 2007) has demonstrated that knock out of the histone demethylase Jhdm2a leads to elevated levels of H3K9me3 in round spermatids, although these changes were undetectable using western blot.

H3.3 is normally depleted for H3K9 methylation (Hake et al., 2006; McKittrick et al., 2004) and is thought to inhibit the spread of heterochromatin, in part through eviction of histones carrying H3K9 methylation (Nakayama et al., 2007). Thus, the gains in the amount of H3K9me3 in *H3f3b* null testes cells might be a direct consequence of decreased H3.3 protein. The H3K9me3

Development (2014) 141, 3483-3494 doi:10.1242/dev.106450

methyltransferase Suv39h2 is most highly expressed in B-type spermatogonia and leptotene spermatocytes and appears to regulate H3K9 methylation at these stages (O'Carroll et al., 2000; Peters et al., 2001), suggesting that the general loss of H3.3 might result in hypermethylation of canonical H3 by Suv39h2. Supporting this hypothesis, H3.3 levels were significantly lower in null germ cell populations where an increased H3K9me3 signal was also observed (supplementary material Fig. S2). Additionally, nucleosome replacement through H3.3 during early pachytene results in a loss of most histone PTMs, leading to the normal *de novo* reappearance of H3K9me3 during stages VI-XII (van der Heijden et al., 2007). We predict that the normal processes by which H3.3 evicts histones bearing repressive PTMs (i.e. H3K9me3) in spermatocytes (Fig. 7A) might be disrupted in null testes, resulting in the overabundance of H3K9me3 (Fig. 7B).

The balance of opened versus closed chromatin during spermiogenesis (Rathke et al., 2013) might also be influenced by H3K9me3, which is involved in chromatin condensation and gene repression (Iwamori et al., 2011; Jenuwein and Allis, 2001; Kouzarides, 2007; Payne and Braun, 2006; Peters et al., 2001). Downregulated genes that are associated with male reproductive function and spermatogenesis in the null testes are normally expressed in round spermatids, suggesting that increased H3K9me3 in round spermatids inhibits their normal development (Fig. 7B). Null sperm also displayed high rates of apoptosis, coinciding with H3K9me3 expression, indicating that this repressive PTM might aberrantly persist throughout spermiogenesis in null testes, leading to sperm death.

Major replacement of nucleoproteins was also disrupted in null testes (supplementary material Fig. S2), as tubules expressing Tnp1 abnormally exhibited characteristics of both the early- and late-stages of spermiogenesis. Further, Prm1 expression was substantially reduced. Decondensed null epididymal sperm exhibited abnormally high levels of H3K9me3 and low levels of Prm1, suggesting that H3K9me3 inhibits the normal reorganization process by which protamines are incorporated into chromatin. These phenotypic effects in nulls could be a consequence of the lost H3K4me3 peaks around protamine and transition protein genes, the expression of which is essential for proper chromatin condensation and protamine replacement during spermiogenesis (Fig. 7A) (Cho et al., 2003; Lee et al., 1995; Okada et al., 2007). Another possibility is that H3.3 loss and H3K9me3 gain alters nucleoprotein exchange, as disruption of nucleoprotein displacement, particularly in regards to replication-independent histone variants (e.g. TH2B) (Montellier et al., 2013) or histone PTMs (Gaucher et al., 2012), can considerably impact the ability of spermatids to properly condense chromatin and incorporate transition proteins or protamines. In this regard, H3.3 plays an important role in chromatin condensation (Lin et al., 2013). In addition to H3.3, the presence of repressive (e.g. H3K27me3) PTMs and chromatin-

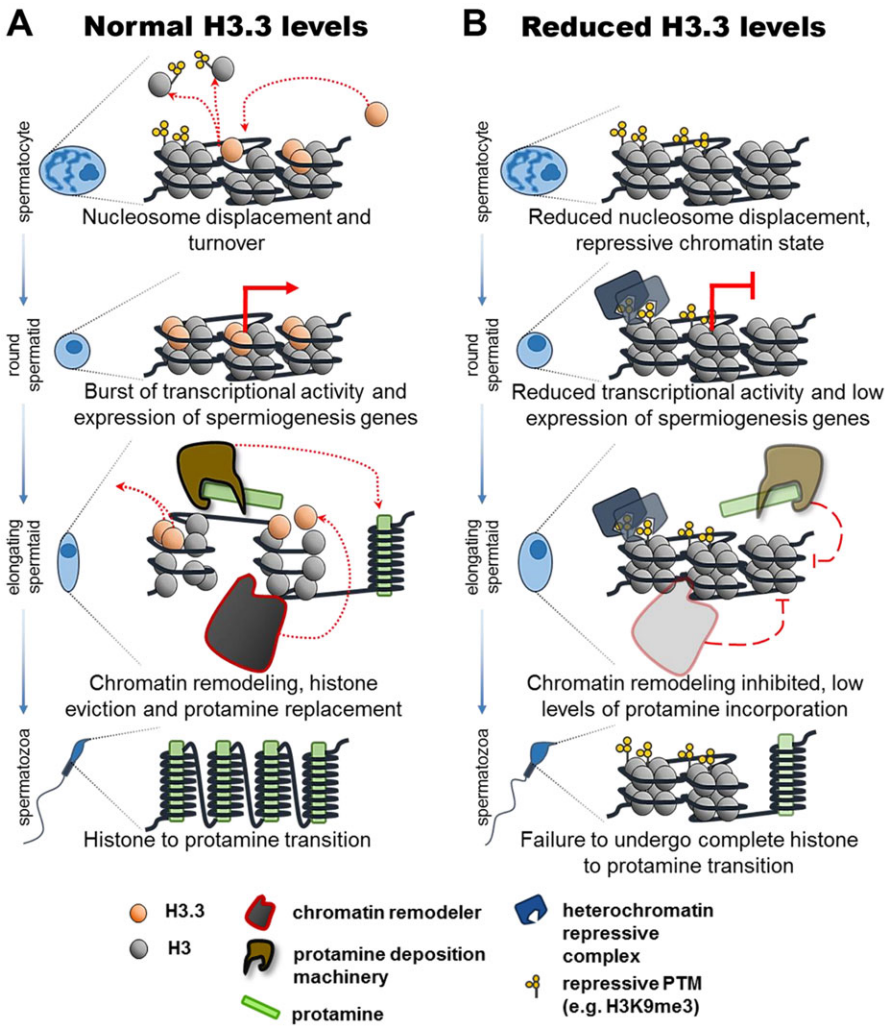

Fig. 7. Model of potential outcomes resulting from H3.3 reduction during spermatogenesis. (A) Normal H3.3 levels allow nucleosome displacement in spermatocytes, resetting many histone PTMs. The presence of sufficient H3.3 also allows for a burst of transcriptional activity in round spermatids, facilitating the transcription of genes required for spermiogenesis, and allows for histone eviction and replacement with protamines. (B) A reduction of H3.3 levels reduces nucleosome turnover in spermatocytes, leading to the accumulation of repressive heterochromatin. Loss of H3.3 also results in lower transcriptional activity and decreased expression of spermiogenesis genes, altering chromatin reorganization dynamics and the transition to protamine.

Development (2014) 141, 3483-3494 doi:10.1242/dev.106450

associated factors contribute to histone retention in protamine-free regions in sperm (Erkek et al., 2013). Taken together, these observations suggest that H3.3 is necessary for normal protamine expression, and further, that the absence of H3.3 and in turn the aberrant presence of repressive PTMs (e.g. H3K9me3) might lead to abnormal chromatin domains in condensing spermatids that block Prm1 deposition in null mice (Fig. 7B).

It is interesting to note that the transcription-coupled incorporation of H3.3 is required to establish marks of active and inactive chromatin that are necessary during fertilization (Erkek et al., 2013); therefore, it might be possible that surviving, null Prm1^{+} spermatozoa face additional problems in activating zygotic transcriptional programs should fertilization occur. The majority of genes with decreased expression were not found in CpG-rich regions, which could suggest that H3.3 plays some regulatory role in maintaining the expression of genes found in CpG-poor areas. Meanwhile, upon H3.3 reduction, the remaining H3.3 histone might be redirected to CpG-rich regions to maintain the function of these genes. Future studies, particularly on *H3f3a*, will further clarify the normal role of histone H3.3 in regulating testes chromatin dynamics and sperm development.

MATERIALS AND METHODS

Animal studies were approved University of California, Davis Institutional Animal Care and Use Committee (IACUC). Additional methods can be found in the supplementary material Methods.

Animals and image analysis

For a comprehensive list of animals used in this study, consult supplementary material Table S1. For a detailed listing on the number of images, cells, testes, or seminiferous tubules used in this study, please consult supplementary material Table S8.

Isolation and immunohistochemistry of testes

Testes (see supplementary material Tables S1, S8) were isolated, embedded in paraffin and specifically treated depending on the antibody (see supplementary material Methods). Primary antibodies against the following proteins were used in this study: H3K9me3 (Abcam 8898), H3K27me3 (Cell Signaling C36B11), H3K4me3 (Millipore 04-745), Tnp1 (Abcam 73135), Prm1 (Briar Patch Biosciences Hup1N), H3 S10P (Millipore 06-570), H3.3 S31P (Abcam ab92628), H3.3 (Abnova H00003021-M01), Sycp3 (from Neil Hunter, UC Davis) and γH2A.X (also from Neil Hunter). Secondary antibodies were used as follows: rabbit or mouse IgG (Alexa488 or Alexa546, Invitrogen) and lectinPNA (Invitrogen L21409). Slides were then mounted using Vectashield mounting medium with DAPI (Vector Labs) and imaged using a Nikon Eclipse 80i microscope (Nikon) with a Retiga 2000R camera (QImaging) or using a Biorevo BZ-9000 microscope system (Keyence).

Testes cell preparation, qPCR and staining analysis for FACS

Testes cell isolation was performed as previously described (Gaysinskaya et al., 2014; Getun et al., 2011) with minor modifications, stained with Hoechst 33342 (Invitrogen #H21492) and propidium iodide (Roche #11348639001), and sorted on a 16 color inFlux v7 high speed cell sorter (Becton-Dickinson-Cytopeia) in a HEPA enclosure. Flow data analysis was performed using FlowJo software (Treestar Incorporated). For qPCR, 75-100% of sorted populations were used for RNA extraction (Macherey-Nagel 740955), concentrated using a Nucleospin RNA XS kit (Macherey-Nagel 740902), and 4-8 ng of RNA was used to amplify cDNA using the CellAmp Whole Transcriptome Amplification Kit (Real Time) Ver. 2 (TaKaRa Biosciences 3734). For staining, sorted cells on slides were treated with antibodies against H3K9me3 (Abcam 8898), Sycp3 and γH2A.X (from Neil Hunter, UC Davis), rabbit or mouse IgG (Alexa488 or Alexa546, Invitrogen), and lectinPNA (Invitrogen L21409) and imaged using a Biorevo BZ-9000 microscope system (Keyence).

WTCL extract, acid extract and western blotting

Whole cell extracts and acid extracts were prepared from one half- to one quarter-testis. Western blotting was performed as described previously (Bush et al., 2013) with a few modifications. Antibodies against the following proteins were used: H3K9me3 (Abcam ab8898), H3K4me3 (Millipore 04-745), β-actin (Sigma A1978), H3.3 (Abnova H00003021-M01), H3.3 S31P (Abcam ab92628), H3K27me3 (Cell Signaling C36B11), H3 (Upstate no. 05-499), anti-rabbit IgG horseradish peroxidase (Jackson 111-035-003), anti-mouse IgG horseradish peroxidase (Jackson 115-035-003), anti-rabbit IgG IRdye800CW (Licor no. 827-08365) and anti-mouse IRdye680RD (Licor no. 926-68170).

qPCR

SYBR Green-based qPCR for genes was performed using Absolute Blue QPCR Master Mix (Thermo Fisher Scientific) and run on a LightCycler 480 (Roche) with included software. Each reaction utilized 10 ng cDNA, and separate reactions containing 10 ng RNA were used to check for genomic DNA contamination. Fold changes were normalized to *Ppia* or *Ubc* and analyzed using the $2^{-\Delta\Delta Ct}$ method.

Microarray and CpG analysis

Microarray analysis was performed on n=2 WT and n=2 null whole testis RNA extracts, as described previously (Bush et al., 2013). RNA from constitutive *H3f3b* null and WT testes was submitted in biological duplicates. A total of 500 ng RNA from each sample was used on an Illumina MouseWG-6 v2 Expression BeadChip containing over 25,000 probes. Amplification and hybridization were performed at the UC Davis Expression Analysis Core according to the Illumina protocol. The data have been deposited with accession number GSE35303 in the GEO database. For CpG analysis, deregulated gene lists were cross-referenced to CpG island tracks on the UCSC Genome Browser and intersected using Galaxy.

ChIP-seq analysis

We conducted ChIP-seq in WT and null testes tissue using two replicates of H3K4me3 (Millipore 04-745) and matched input controls. Tissue preparation and ChIP were performed as described previously (Barrilleaux et al., 2013). Libraries were prepared as described previously (Bush et al., 2013) and sequenced using an Illumina HiSeq, yielding at least 6 million reads per sample (supplementary material Table S5). The data have been deposited with the accession number GSE60207 in the GEO database.

Seminiferous tubule staging, quantification and Cenpa analysis

Staging of mouse seminiferous tubules was performed as described previously (Ahmed and de Rooij, 2009; Hess and Renato de Franca, 2008; Meistrich and Hess, 2013) using lectinPNA acrosomal staining as a guide. For quantification of meiotic tubules, meiotic spermatocytes and spermatids, testes were stained with an antibody against H3 S10P (Millipore 06-570), lectinPNA (Invitrogen L21409) or lectinPNA alone. Staged tubules were then quantified for the presence of H3 S10P^{+} tubules and H3 S10P^{+} cells or round (step 1) and elongated (step 13) spermatids.

Sperm assessment and staining

Male animals were submitted to the UC Davis Mouse Biology Program for sperm functional testing. Sperm were isolated using the swim-out method from the epididymis and assessed using an IVOS computerized sperm analyzer (Hamilton Thorne). Approximately 5×10^{6} spermatozoa were placed on slides, decondensed, stained and imaged using a Biorevo BZ-9000 microscope system (Keyence).

TUNEL staining and quantification

Paraffin-embedded testes sections or spermatozoa slides were used for TUNEL staining (DeadEnd Fluorometric TUNEL System, Promega G3250). TUNEL^{+} tubules were counted when exhibiting one or more apoptotic events. Quantification of apoptotic nuclei was performed using ImageJ software.

Development (2014) 141, 3483-3494 doi:10.1242/dev.106450

Statistical analysis

Student's two-tailed, unpaired *t*-tests were used to determine significance between null and WT animal measurements. *P*-values for Venn diagram overlaps were calculated in R using the hypergeometric test. Error bars represent s.e.m. unless otherwise noted.

Acknowledgements

We thank the UC Davis Mouse Biology Program for aid in production of the targeted *H3f3b* mice and sperm analysis and Stephen Griffey and Amanda Koehne for analysis of the knockout mice organ histology. We thank the UC Davis Expression Analysis and DNA Technologies Cores for their assistance with expression array studies and sequencing support, and Jonathan Van Dyke from the UC Davis Flow Cytometry Facility for his assistance and expertise. We thank Rod Balhorn for advice on testes analysis, Henriette O'Geen for aid in ChIP-Seq studies, Neil Hunter for advice and antibodies, and Richard Yan for performing blinded seminiferous tubule quantification and analysis.

Competing interests

The authors declare no competing financial interests.

Author contributions

B.T.K.Y. performed the majority of the experiments reported: testes and sperm IHC-IF staining and analysis; sperm imaging and analysis; FACS sorting and analysis; western blotting and quantification; tubule and TUNEL staining, analysis and staging; microarray analysis; CENPA staining and quantification; qPCR; and data preparation and interpretation. K.M.B. performed TUNEL staining, qPCR, the majority of the western blotting, prepared RNA for microarrays, and conducted all mouse breeding and genotyping. B.L.B. performed ChIP-seq data analysis. R.C. prepared ChIP samples. P.S.K. conceived the project, supervised the studies, and along with B.T.K.Y., conducted experimental design and data interpretation. B.T.K.Y. wrote the manuscript. B.T.K.Y., P.S.K., K.M.B., B.L.B. and R.C. read, edited and approved the manuscript.

Funding

This work was supported by a National Institutes of Health grant [5K01CA114400-05] and a California Institute for Regenerative Medicine (CIRM) grant [RN2-00922-1], both to P.K.; and in part by grants made possible from the UC Davis Howard Hughes Medical Institute: Integrating Medicine into Basic Science Program [grant 56006769] and the CIRM Stem Cell Training Program [CIRM grant TG2-01163] to B.T.K.Y. Deposited in PMC for release after 12 months.

Supplementary material

Supplementary material available online at
http://dev.biologists.org/lookup/suppl/doi:10.1242/dev.106450/-/DC1

References

Ahmad, K. and Henikoff, S. (2002). The histone variant H3.3 marks active chromatin by replication-independent nucleosome assembly. *Mol. Cell* **9**, 1191-1200.

Ahmed, E. A. and de Rooij, D. G. (2009). Staging of mouse seminiferous tubule cross-sections. *Methods Mol Biol* **558**, 263-77.

Akhmanova, A. S., Bindels, P. C. T., Xu, J., Miedema, K., Kremer, H. and Hennig, W. (1995). Structure and expression of histone H3.3 genes in *Drosophila melanogaster* and *Drosophila hydei*. *Genome* **38**, 586-600.

Aviles, M., Castells, M. T., Martinez-Menarguez, J. A., Abascal, I. and Ballesta, J. (1997). Localization of penultimate carbohydrate residues in zona pellucida and acrosomes by means of lectin cytochemistry and enzymatic treatments. *Histochem. J.* **29**, 583-592.

Balhorn, R. (2007). The protamine family of sperm nuclear proteins. *Genome Biol.* **8**, 227.

Barrilleaux, B. L., Cotterman, R. and Knoepfler, P. S. (2013). Chromatin immunoprecipitation assays for myc and N-myc. *Methods Mol. Biol.* **1012**, 117-133.

Bastos, H., Lassalle, B., Chicheportiche, A., Riou, L., Testart, J., Allemand, I. and Fouchet, P. (2005). Flow cytometric characterization of viable meiotic and postmeiotic cells by Hoechst 33342 in mouse spermatogenesis. *Cytometry A* **65**, 40-49.

Bordlein, A., Scherthan, H., Nelkenbrecher, C., Molter, T., Bosl, M. R., Dippold, C., Birke, K., Kinkley, S., Staege, H. and Will, H. et al. (2011). SPOC1 (PHF13) is required for spermatogonial stem cell differentiation and sustained spermatogenesis. *J. Cell Sci.* **124**, 3137-3148.

Bramlage, B., Kosciessa, U. and Doenecke, D. (1997). Differential expression of the murine histone genes H3.3A and H3.3B. *Differentiation* **62**, 13-20.

Braun, R. E. (2001). Packaging paternal chromosomes with protamine. *Nat. Genet.* **28**, 10-12.

Bush, K. M., Yuen, B. T. K., Barrilleaux, B. L., Riggs, J. W., O'Geen, H., Cotterman, R. F. and Knoepfler, P. S. (2013). Endogenous mammalian histone H3.3 exhibits chromatin-related functions during development. *Epigenetics Chromatin* **6**, 7.

Carrell, D. T., Emery, B. R. and Hammoud, S. (2007). Altered protamine expression and diminished spermatogenesis: what is the link? *Hum. Reprod. Update* **13**, 313-327.

Chen, H. Y., Sun, J.-M., Zhang, Y., Davie, J. R. and Meistrich, M. L. (1998). Ubiquitination of histone H3 in elongating spermatids of rat testes. *J. Biol. Chem.* **273**, 13165-13169.

Cheng, C. Y. and Mruk, D. D. (2012). The blood-testis barrier and its implications for male contraception. *Pharmacol. Rev.* **64**, 16-64.

Cho, C., Jung-Ha, H., Willis, W. D., Goulding, E. H., Stein, P., Xu, Z., Schultz, R. M., Hecht, N. B. and Eddy, E. M. (2003). Protamine 2 deficiency leads to sperm DNA damage and embryo death in mice. *Biol. Reprod.* **69**, 211-217.

Couldrey, C., Carlton, M. B. L., Nolan, P. M., Colledge, W. H. and Evans, M. J. (1999). A retroviral gene trap insertion into the histone 3.3A gene causes partial neonatal lethality, stunted growth, neuromuscular deficits and male sub-fertility in transgenic mice. *Hum. Mol. Genet.* **8**, 2489-2495.

Erkek, S., Hisano, M., Liang, C.-Y., Gill, M., Murr, R., Dieker, J., Schübeler, D., van der Vlag, J., Stadler, M. B. and Peters, A. H. F. M. (2013). Molecular determinants of nucleosome retention at CpG-rich sequences in mouse spermatozoa. *Nat. Struct. Mol. Biol.* **20**, 868-875.

Gaucher, J., Boussouar, F., Montellier, E., Curtet, S., Buchou, T., Bertrand, S., Hery, P., Jounier, S., Depaux, A. and Vitte, A.-L. et al. (2012). Bromodomain-dependent stage-specific male genome programming by Brdt. *EMBO J.* **31**, 3809-3820.

Gaysinskaya, V., Soh, I. Y., van der Heijden, G. W. and Bortvin, A. (2014). Optimized flow cytometry isolation of murine spermatocytes. *Cytometry A* **85**, 556-565.

Getun, I. V., Torres, B. and Bois, P. R. (2011). Flow cytometry purification of mouse meiotic cells. *J. Vis. Exp.* **50**, e2602.

Godmann, M., Auger, V., Ferraroni-Aguiar, V., Di Sauro, A., Sette, C., Behr, R. and Kimmins, S. (2007). Dynamic regulation of histone H3 methylation at lysine 4 in mammalian spermatogenesis. *Biol. Reprod.* **77**, 754-764.

Hake, S. B., Garcia, B. A., Duncan, E. M., Kauer, M., Dellaire, G., Shabanowitz, J., Bazett-Jones, D. P., Allis, C. D. and Hunt, D. F. (2006). Expression patterns and post-translational modifications associated with mammalian histone H3 variants. *J. Biol. Chem.* **281**, 559-568.

Hammoud, S. S., Nix, D. A., Zhang, H., Purwar, J., Carrell, D. T. and Cairns, B. R. (2009). Distinctive chromatin in human sperm packages genes for embryo development. *Nature* **460**, 473-478.

Hess, R. A. and Renato de Franca, L. (2008). Spermatogenesis and cycle of the seminiferous epithelium. *Adv. Exp. Med. Biol.* **636**, 1-15.

Hödl, M. and Basler, K. (2009). Transcription in the absence of histone H3.3. *Curr. Biol.* **19**, 1221-1226.

Huang da, W., Sherman, B. T. and Lempicki, R. A. (2009a). Bioinformatics enrichment tools: paths toward the comprehensive functional analysis of large gene lists. *Nucleic Acids Res.* **37**, 1-13.

Huang da, W., Sherman, B. T. and Lempicki, R. A. (2009b). Systematic and integrative analysis of large gene lists using DAVID bioinformatics resources. *Nat. Protoc.* **4**, 44-57.

Iwamori, N., Zhao, M., Meistrich, M. L. and Matzuk, M. M. (2011). The testis-enriched histone demethylase, KDM4D, regulates methylation of histone H3 lysine 9 during spermatogenesis in the mouse but is dispensable for fertility. *Biol. Reprod.* **84**, 1225-1234.

Jenuwein, T. and Allis, C. D. (2001). Translating the histone code. *Science* **293**, 1074-1080.

Jin, C., Zang, C., Wei, G., Cui, K., Peng, W., Zhao, K. and Felsenfeld, G. (2009). H3.3/H2A.Z double variant-containing nucleosomes mark 'nucleosome-free regions' of active promoters and other regulatory regions. *Nat. Genet.* **41**, 941-945.

Korhonen, H. M., Meikar, O., Yadav, R. P., Papaioannou, M. D., Romero, Y., Da Ros, M., Herrera, P. L., Toppari, J., Nef, S. and Kotaja, N. (2011). Dicer is required for haploid male germ cell differentiation in mice. *PLoS ONE* **6**, e24821.

Kouzarides, T. (2007). Chromatin modifications and their function. *Cell* **128**, 693-705.

Lee, K., Haugen, H. S., Clegg, C. H. and Braun, R. E. (1995). Premature translation of protamine 1 mRNA causes precocious nuclear condensation and arrests spermatid differentiation in mice. *Proc. Natl. Acad. Sci. USA* **92**, 12451-12455.

Lewis, J. D., Abbott, D. W. and Ausió, J. (2003). A haploid affair: core histone transitions during spermatogenesis. *Biochem. Cell Biol.* **81**, 131-140.

Lin, C.-J., Conti, M. and Ramalho-Santos, M. (2013). Histone variant H3.3 maintains a decondensed chromatin state essential for mouse preimplantation development. *Development* **140**, 3624-3634.

Liu, Z., Zhou, S., Liao, L., Chen, X., Meistrich, M. and Xu, J. (2010). Jmjd1a demethylase-regulated histone modification is essential for cAMP-response element modulator-regulated gene expression and spermatogenesis. *J. Biol. Chem.* **285**, 2758-2770.

Martins, R. P. and Krawetz, S. A. (2007). Decondensing the protamine domain for transcription. *Proc. Natl. Acad. Sci. USA* **104**, 8340-8345.

McKittrick, E., Gafken, P. R., Ahmad, K. and Henikoff, S. (2004). Histone H3.3 is enriched in covalent modifications associated with active chromatin. *Proc. Natl. Acad. Sci. USA* **101**, 1525-1530.
Meistrich, M. L. and Hess, R. A. (2013). Assessment of spermatogenesis through staging of seminiferous tubules. *Methods Mol. Biol.* **927**, 299-307.
Miller, D., Brinkworth, M. and Iles, D. (2010). Paternal DNA packaging in spermatozoa: more than the sum of its parts? DNA, histones, protamines and epigenetics. *Reproduction* **139**, 287-301.
Montellier, E., Boussouar, F., Rousseaux, S., Zhang, K., Buchou, T., Fenaille, F., Shiota, H., Debernardi, A., Hery, P. and Curtet, S. et al. (2013). Chromatin-to-nucleoprotamine transition is controlled by the histone H2B variant TH2B. *Genes Dev.* **27**, 1680-1692.
Morales, A., Mohamed, F. and Cavicchia, J. C. (2007). Apoptosis and blood-testis barrier during the first spermatogenic wave in the pubertal rat. *Anat. Rec. (Hoboken)* **290**, 206-214.
Mruk, D. D. and Cheng, C. Y. (2004). Sertoli-Sertoli and Sertoli-germ cell interactions and their significance in germ cell movement in the seminiferous epithelium during spermatogenesis. *Endocr. Rev.* **25**, 747-806.
Nakayama, T., Nishioka, K., Dong, Y.-X., Shimojima, T. and Hirose, S. (2007). Drosophila GAGA factor directs histone H3.3 replacement that prevents the heterochromatin spreading. *Genes Dev.* **21**, 552-561.
Oishi, K., Barchi, M., Au, A. C., Gelb, B. D. and Diaz, G. A. (2004). Male infertility due to germ cell apoptosis in mice lacking the thiamin carrier, Tht1. A new insight into the critical role of thiamin in spermatogenesis. *Dev. Biol.* **266**, 299-309.
Okada, Y., Scott, G., Ray, M. K., Mishina, Y. and Zhang, Y. (2007). Histone demethylase JHDM2A is critical for Tnp1 and Prm1 transcription and spermatogenesis. *Nature* **450**, 119-123.
O'Carroll, D., Scherthan, H., Peters, A. H. F. M., Opravil, S., Haynes, A. R., Laible, G., Rea, S., Schmid, M., Lebersorger, A. and Jerratsch, M. et al. (2000). Isolation and characterization of Suv39h2, a second histone H3 methyltransferase gene that displays testis-specific expression. *Mol. Cell. Biol.* **20**, 9423-9433.
Payne, C. and Braun, R. E. (2006). Histone lysine trimethylation exhibits a distinct perinuclear distribution in Plzf-expressing spermatogonia. *Dev. Biol.* **293**, 461-472.
Peters, A. H. F. M., O'Carroll, D., Scherthan, H., Mechtler, K., Sauer, S., Schöfer, C., Weipoltshammer, K., Pagani, M., Lachner, M. and Kohlmaier, A. et al. (2001). Loss of the Suv39h histone methyltransferases impairs mammalian heterochromatin and genome stability. *Cell* **107**, 323-337.
Rathke, C., Baarends, W. M., Awe, S. and Renkawitz-Pohl, R. (2013). Chromatin dynamics during spermiogenesis. *Biochim. Biophys. Acta.* **1839**, 155-168.
Ray-Gallet, D., Woolfe, A., Vassias, I., Pellentz, C., Lacoste, N., Puri, A., Schultz, D. C., Pchelintsev, N. A., Adams, P. D. and Jansen, L. E. et al. (2011). Dynamics of histone H3 deposition in vivo reveal a nucleosome gap-filling mechanism for H3.3 to maintain chromatin integrity. *Mol. Cell* **44**, 928-941.
Sakai, A., Schwartz, B. E., Goldstein, S. and Ahmad, K. (2009). Transcriptional and developmental functions of the H3.3 histone variant in Drosophila. *Curr. Biol.* **19**, 1816-1820.
Szasz, F., Sirivaidyapong, S., Cheng, F. P., Voorhout, W. F., Marks, A., Colenbrander, B. and Solti, B. M. (2000). Detection of calcium ionophore induced membrane changes in dog sperm as a simple method to predict the cryopreservability of dog semen. *Mol. Reprod. Dev.* **55**, 289-298.
Szenker, E., Ray-Gallet, D. and Almouzni, G. (2011). The double face of the histone variant H3.3. *Cell Res.* **21**, 421-434.
Tachibana, M., Nozaki, M., Takeda, N. and Shinkai, Y. (2007). Functional dynamics of H3K9 methylation during meiotic prophase progression. *EMBO J.* **26**, 3346-3359.
Tagami, H., Ray-Gallet, D., Almouzni, G. and Nakatani, Y. (2004). Histone H3.1 and H3.3 complexes mediate nucleosome assembly pathways dependent or independent of DNA synthesis. *Cell* **116**, 51-61.
Tan, M., Luo, H., Lee, S., Jin, F., Yang, J. S., Montellier, E., Buchou, T., Cheng, Z., Rousseaux, S. and Rajagopal, N. et al. (2011). Identification of 67 histone marks and histone lysine crotonylation as a new type of histone modification. *Cell* **146**, 1016-1028.
Tang, M. C. W., Jacobs, S. A., Wong, L. H. and Mann, J. R. (2013). Conditional allelic replacement applied to genes encoding the histone variant H3.3 in the mouse. *Genesis* **51**, 142-146.
van der Heijden, G. W., Derijck, A. A. H. A., Ramos, L., Giele, M., van der Vlag, J. and de Boer, P. (2006). Transmission of modified nucleosomes from the mouse male germline to the zygote and subsequent remodeling of paternal chromatin. *Dev. Biol.* **298**, 458-469.
van der Heijden, G. W., Derijck, A. A. H. A., Pósfai, E., Giele, M., Pelczar, P., Ramos, L., Wansink, D. G., van der Vlag, J., Peters, A. H. F. M. and de Boer, P. (2007). Chromosome-wide nucleosome replacement and H3.3 incorporation during mammalian meiotic sex chromosome inactivation. *Nat. Genet.* **39**, 251-258.
Witt, O., Albig, W. and Doenecke, D. (1997). Transcriptional regulation of the human replacement histone gene H3.3B. *FEBS Lett.* **408**, 255-260.
Yu, Y. E., Zhang, Y., Unni, E., Shirley, C. R., Deng, J. M., Russell, L. D., Weil, M. M., Behringer, R. R. and Meistrich, M. L. (2000). Abnormal spermatogenesis and reduced fertility in transition nuclear protein 1-deficient mice. *Proc. Natl. Acad. Sci. USA* **97**, 4683-4688.
Zhao, M., Shirley, C. R., Mounsey, S. and Meistrich, M. L. (2004). Nucleoprotein transitions during spermiogenesis in mice with transition nuclear protein Tnp1 and Tnp2 mutations. *Biol. Reprod.* **71**, 1016-1025.
Zheng, J., Xia, X., Ding, H., Yan, A., Hu, S., Gong, X., Zong, S., Zhang, Y. and Sheng, H. Z. (2008). Erasure of the paternal transcription program during spermiogenesis: the first step in the reprogramming of sperm chromatin for zygotic development. *Dev. Dyn.* **237**, 1463-1476.

Supplemental Methods

Animals and image analysis

For a listing of animals used in this study, and mean/median age ranges, please consult Table S1. All animals in this study were in the C57BL/6 genetic background, which does not display a subfertile phenotype. Null males (n = 4) failed to produce any offspring when mated to WT females for ≥ 4 months. *H3f3b* heterozygotes and WT males were able to produce offspring without noticeable differences. For a detailed listing on the number of images, cells, testes, or seminiferous tubules analyzed for different staining protocols in this study, please consult Table S8.

Isolation and immunohistochemistry of testes

Deparaffinization was performed as follows: 3 X 5 min washes in xylene, 1 X 3 min wash in xylene:100% ethanol (1:1), 2 X 3 min washes in 100% ethanol, 1 X 3 min wash in 95% ethanol, 1 X 3 min wash in 80% ethanol, 1 X 3 min wash in 50% ethanol, 1 X 3 min wash in dH2O, followed by a final 10 min wash in dH2O. Heat-induced epitope retrieval was performed as follows: deparaffinized slides were added to preheated (95°C) sodium citrate buffer (10 mM sodium citrate, 0.05% Tween-20, pH 6.0), and incubated for 40 min. Slides were then removed and kept in sodium citrate buffer for a 15 min cool-down period, and then transferred to 1 X Tris-buffered saline (TBS, 50 mM Tris-Cl, 150 mM NaCl) for 10 min. Depending on the antibody, a few additional steps were taken. For H3K9me3, H3K4me3, Prm1, TP1, H3pS10, lectinPNA, and H3.3 antibodies, slides were incubated with 10 mM DTT in TBS for 120 min, followed by a 1 X 5 min wash in TBS. Slides were then permeabilized with 2% Triton X-100 for 30 min, and then washed 1 X 5 min with TBS. For the H3.3 antibody slides, this was also followed by a 90 min incubation with 0.4 units/µL DNase I (Sigma D4527) solution in TBS. DNase I was then washed off slides with 1 X 5 min TBS. Slides for H3K9me3, H3K4me3, lectinPNA, and H3pS10 antibodies were also processed (separately) without DTT treatment, which did not noticeably affect staining intensity. Slides were then blocked for 30 min in 10% normal goat serum in TBS, followed by a brief rinse in TBS. Primary antibodies for H3K9me3 (Abcam 8898, 1:200), H3K27me3 (Cell Signaling C36B11, 1:200), H3K4me3 (Millipore 04-745, 1:200), TP1 (Abcam 73135, 1:200), Prm1/Hup1N (Briar Patch Biosciences Hup1N, 1:100), H3 S10P (Millipore 06-570, 1:200), H3.3 S31P (Abcam ab92628, 1:200), H3.3 (Abnova H00003021-M01, 1:80), Sycp3 (from Dr. Neil Hunter, UC Davis, 1:500), and γH2A.X (also from Dr. Hunter, 1:300). were diluted in carrier solution (1% BSA in TBS) and incubated on sections at 4°C overnight. Slides were then washed 3 X 5 min each with 0.025% Triton X-100 in TBS.

Secondary antibodies for rabbit or mouse IgG (Alexa488 or Alexa546, Invitrogen, 1:200) and LectinPNA (Invitrogen L21409, 1:100).were diluted in carrier solution and applied for 90 min at room temperature (RT), then washed 3 X 5 min with TBS. Slides were then mounted and imaged.

Testes cell isolation and preparation for flow associated cell sorting (FACS)

Testes cell isolation was performed as described in (Gaysinskaya et al., 2014; Getun et al., 2011) with modifications. Two decapsulated testes were placed in 6 mL of Gey's balanced salt solution (GBSS) supplemented with 200 U/mL of collagenase type IV (Gibco #17104-019) and 20 ug of DNase I (StemCell Technologies #07900, 1 mg/mL stock) and were digested for 15 min at 33°C, 120 rpm. Seminiferous tubules were precipitated by vertical standing at RT for 1 min. Interstitial cells were decanted, and the digestion process was repeated an additional time. Seminiferous tubules were then digested in 5 mL of GBSS supplemented with 200 U/mL of collagenase type IV, 20 µg of DNase I, and 500 µg of trypsin (Gibco #15090, 25 mg/mL stock) for 15 min at 33°C, 120 rpm. Tubules were then broken up by gentle pipetting for 3 min using plastic transfer pipettes (Fisher #13-711-9AM). At this point, 60 µg trypsin and 20 µg DNase I were added, and cells were stained with freshly made 80 µg Hoechst 33342 (Invitrogen #H21492) resuspended in DMSO (10 mg/mL). Cells were then incubated for 15 min at 33°C, 120 rpm. 1 mL of fetal bovine serum was then added to inactivate the trypsin. Final staining Hoechst staining was done by adding 100 µg of Hoechst 33342 and 20 µg of DNase I, and incubated for an additional 15 min at 33°C, 120 rpm. Samples were then passed through two successive 40 µm filters and protected from light until FACS. Cells were stained with 250 µL propidium iodide (PI) (Roche #11348639001, 0.5 mg/mL) immediately before processing.

FACS and flow cytometry data analysis

Samples (See Table S1) were run on a 16 color inFlux v7 high speed cell sorter (Becton-Dickinson-Cytopeia) in a HEPA enclosure. The flow rate was adjusted to roughly 8,000 events/second. Cells were sorted into DMEM (Gibco #11960-044) supplemented with 10% FBS (HyClone #SH30396-03), 1X non-essential amino acids (Corning #25-025-Cl), and 1X penicillin-streptomycin/L-glutamine (JR Scientific #20020) and kept on ice. Hoechst33342 fluorescence was captured using a UV (355 nm) laser, with a 460/50 nm pass for Hoechst blue detection and a 670/30 nm pass for Hoechst red detection; PI fluorescence was captured using a 532 nm laser, with a 610/20 nm pass for PI detection. For flow data acquisition, 500,000 events were recorded during the sort for downstream

analysis (200,000 for null sample NL#4242). Flow data analysis was performed using FlowJo software (Treestar Incorporated).

Staining of FACS-sorted cells

Sorted cells on slides (see Table S1 for animals used) were kept at -80°C prior to use. Cells were brought to room temperature, and then immediately fixed for 10 min in ice-cold 100% methanol. Cells were then washed 3 X 5 min in TBS, then permeabilized in 0.5% Triton X-100:TBS for 10 min. Cells were then washed 3 X 5 min in TBS, then blocked in 10% normal goat serum for 1 hour. Prior to primary antibody incubation, cells were washed 1 X 5 min in TBS, and primary antibody in carrier solution (1% BSA in TBS) was added to cells overnight at 4°C. Cells were then washed 3 X 5 min in 0.025% Triton X-100:TBS, and then stained with secondary antibody in carrier solution for 1-2 hours at room temperature. Slides were then washed 3 X 5 min in 0.025% Triton X-100 and mounted using Vectashield mounting medium with DAPI (Vector Labs). Slides were imaged using a Biorevo BZ-9000 microscope system (Keyence). The following antibodies were used: H3K9me3 (Abcam 8898, 1:200), Sycp3 (from Dr. Neil Hunter, UC Davis, 1:500), and γH2A.X (also from Dr. Hunter, 1:300), rabbit or mouse IgG (Alexa488 or Alexa546, Invitrogen, 1:200), and LectinPNA (Invitrogen L21409, 1:100).

Whole cell testes lysate extract, acid extract, and Western blotting

Whole cell extracts were prepared by digesting one half-testis with RIPA buffer (50 mM Tris HCl [pH 8.0], 150 mM NaCl, 1% NP-40, 0.5% Sodium Deoxycholate, 0.1% SDS and Roche complete midi protease inhibitors [Catalog #11836170001]) and dounce homogenizing on ice. Samples were incubated on ice for 30 min and sonicated on high for one minute, or until samples were homogenous and clear. Samples were then aliquoted and frozen at -80°C. For acid extraction, one quarter to one half testis were digested with trypsin (JR Scientific #82702) and diced with sterile razorblades for 5 min. The reaction was then neutralized by the addition of DMEM (Gibco #11960-044) supplemented with 10% FBS (HyClone #SH30396-03), 1X non-essential amino acids (Corning #25-025-Cl), and 1X penicillin-streptomycin/L-glutamine (JR Scientific #20020). Samples were immediately stored on ice, spun down at 200 x g for 3 min, and washed 2X in PBS supplemented with 5 mM sodium butyrate. Cells were then resuspended in Triton extraction buffer (TEB) containing 0.5% Triton X-100, 2 mM phenylmethylsulfonyl fluoride, and 0.02% (w/v) NaN_3 in sodium butyrate-supplemented PBS at a cell density of roughly 1 x 10^7 cells per mL for 5

min on ice with dounce homogenization. Nuclei were then centrifuged at 6,500 x g for 10 min at 4°C, and the supernatant was discarded. Nuclei were then washed in half the volume of TEB and re-centrifuged. Histones were then extracted from nuclei using ice cold 0.2 N HCl in one quarter of the volume from the prior TEB wash, and incubated overnight at 4°C. Samples were then spun down at 6,500 x g for 10 min at 4°C, neutralized with 1 N NaOH, aliquoted, and flash frozen in liquid nitrogen and stored at -80°C. Equivalent levels of protein were run through 6-12% Bis-Tris gel as indicated by Invitrogen protocol. Protein was then transferred onto PVDF membrane, and two methods were used for detection: chemiluminescence (ECL) or infrared (IR) conjugated antibody. For ECL, membranes were blocked 1 hour in 5% milk; for IR, membranes were blocked 1 hour with Odyssey blocking buffer (Licor 927-40100). Two methods were employed when incubating western blots with primary antibodies. Membranes were either (1) blocked one hour in 5% milk/TBST (for ECL) or Odyssey blocking buffer (for IR) at RT and then incubated in primary overnight at 4°C, or (2) blocked overnight at 4°C in 5% milk/TBST (for ECL) then incubated with primary for two hours at RT. The following antibodies were used: H3K9me3 (Abcam ab8898, 1:2000), H3K4me3 (Millipore 04-745, 1:5000), β-actin (Sigma A1978, 1:8000), H3.3 (Abnova H00003021-M01, 1:50), H3.3 S31P (Abcam ab92628, 1:2000), H3K27me3 (Cell Signaling C36B11, 1:1000), H3 (Upstate #05-499, 1:1000), anti-rabbit HRP (Jackson 111-035-003, 1:4000), anti-mouse HRP (Jackson 115-035-003, 1:4000), anti-rabbit IRdye800CW (Licor #827-08365, 1:10,000), anti-mouse IRdye680RD (Licor #926-68170, 1:10,000). All secondary antibodies were applied for 1 hour at RT. Western blot quantification was performed using multiple high-resolution exposures in ImageJ software (for ECL) (http://rsb.info.nih.gov/ij/) or using an Odyssey CLx system (for IR) (Licor). WT (WT#1, WT#4) and null (NL#2-3, NL#5) acid extracts were blotted n = 6 times and combined for analysis.

qPCR

The following primers were used: *Sna1* F, 5′-CTCACCTCGGGAGCATACAG-3′, R, 5′-GACTTACACGCCCCAAGGATG-3′; *Gpt2* F, 5′-TGAAGCTACTCTCGGTTCGC-3′, R, 5′-CACTGGATCCCTGGGACTTG-3′; *Prkra* F, 5′-ACGAGTACGGCATGAAGACC-3′, R, 5′-GCTTCGCCAGCTTCTTACTTG-3′; *Hk1* F, 5′-CACCGGCAGATTGAGGAAAC-3′, R, 5′-CTCAGCCCCATTTCCATCTCT-3′; *Catsper3* F, 5′-GAGTGCCAGGCTTACTTCAGG-3′, 5′-GGAACTCGCAGACATAGACAGA-3′; *Lrcc52* F, 5′-GTACCTAAGTGGGAACCCCTG-3′, R, 5′-

ATGCACATGTACTGGAGTGGA-3′; *Catsper1* F, 5′-GCAAGCTGCCCGGGTCCATGA-3′, R, 5′-GAACTGGAAGTGGAGCACCCGC-3′; *Hook1* F, 5′-ACGCAGCTCGGGCACAGTTA-3′, R, 5′-CCGCAGCTCCTCATTCGTCTCC-3′; *Spaca3* F, 5′-CCACCGCTGTCATCGTCCCC-3′, R, 5′-ATAGGCCAGGGCCAGCCAAGT-3′; *Adig/BC054059* F, 5′-TTCAACTGGGAGCCCTGGAGCA-3′, R, 5′-AGGGAAGGCCATCGGTCACCA-3′; *Ubc* F, 5′-AGCCCAGTGTTACCACCAAG-3′, R, 5′-CTAAGACACCTCCCCCATCA-3′; *Prm1* F, 5′-GAAGATGTCGCAGACGGAGG-3′, R, 5′-CGGACGGTGGCATTTTTCAA-3′; *Prm2* F, 5′-CATAGGATCCACAAGAGGCGT-3′, R, 5′-GCTTAGTGATGGTGCCTCCT-3′; *Prm3* F, 5′-GTGAGTCAAGACAACTTTTCCCTG-3′, R, 5′-GAGTGTGTCTGCTTGGGCTC-3′; *Tnp1* F, 5′-TCACAAGGGCGTCAAGAGAG-3′, R, 5′-GCATCACAAGTGGGATCGGT-3′; *Tnp2* F, 5′-TCGACACTCACCTGCAAGAC-3′, R, 5′-ATCCTGGAGTGCGTCACTTG-3′; *Ppia* F, 5′-CAGACGCCACTGTCGCTTT-3′, R, 5′-TGTCTTTGGAACTTTGTCTGCAA-3′. For FACS-sorted cells, following the cell sort, 75-100% of FACS-sorted populations were used for RNA extraction (Macherey-Nagel 740955). RNA was then concentrated using a Nucleospin RNA XS kit (Macherey-Nagel 740902) and 4-8 ng of RNA was used to generate and amplify cDNA using the CellAmp Whole Transcriptome Amplification Kit (Real Time) Ver. 2 (TaKaRa Biosciences 3734). qPCR analysis was performed using Absolute Blue QPCR Master Mix (Thermo Fisher Scientific) and run on a LightCycler 480 (Roche) with included software. Each reaction utilized 2.5 ng cDNA.

Microarray and CpG analysis

Microarray data were analyzed using GenomeStudio version 3.1.1.0 (Illumina) and data deposited as GSE35303 in the GEO database (http://www.ncbi.nlm.nih.gov/geo/). Analysis of online transcriptomic data was performed as in (Gaucher et al., 2012; Tan et al., 2011) using GEO studies GSE21749 (4 samples), GSE4193 (8 samples), GSE23119 (3 samples), and GSE21447 (20 samples). Affymetrix Array 430 2.0 expression data (.CEL files) were downloaded and analyzed using R/Bioconductor (Gentleman et al., 2004). Datasets were normalized by robust multi-array average (RMA) using the "oligo" R package (Carvalho and Irizarry, 2010), and heatmap images were generated using the "gplots" and "RColorBrewer" R packages. For CpG analysis, deregulated gene lists containing genes up- or downregulated by 1.5-fold or more (see Table S3) were cross-referenced to their Illumina Probe identifiers and RefSeq symbols and corresponding genomic coordinates using the UCSC Genome Browser (Kent et

al., 2002). CpG island (CGI) tracks (Unmasked CpG) were generated using Galaxy and the UCSC Genome Browser for CpG observed/expected ratios in three ranges: CpG O/E > 0.8, CpG O/E 0.6-0.8, and CpG O/E < 0.6 (Gardiner-Garden and Frommer, 1987; Mohn et al., 2008). Galaxy was then used to intersect CGI tracks and gene lists.

ChIP-seq analysis

Reads were aligned to the mm9 mouse genome using Bowtie (Langmead et al., 2009), followed by peak calling with HOMER (Heinz et al., 2010) using the default settings for histone peaks. We used the R package DiffBind to identify significantly changed ChIP-seq peaks (Ross-Innes et al., 2012). The Peak2Gene tool in Galaxy Cistrome was used to identify genes near peaks, and DAVID was used for gene ontology analysis. Major and minor satellite repeat sequences (GSAT_MM and SATMIN in RepBase notation) were identified in 650,000 ChIP-seq reads per sample (H3K4me3 ChIP or input) using RepeatMasker. Tag counts in H3K4me3 were normalized to counts in matched input samples. H3K4me3 ChIP-seq profiles were plotted using the UCSC Genome Browser (Kent et al., 2002).

Staging of mouse seminiferous tubules

Staging of mouse seminiferous tubules was performed as described (Ahmed and de Rooij, 2009; Hess and Renato de Franca, 2008; Meistrich and Hess, 2013) using LectinPNA acrosomal staining as a guide. Stage I was defined by the presence of two generations of spermatids (round and elongated) and no acrosomal granules present in round spermatids. Stage II-III were defined by the presence of two generations of spermatids, and the presence of acrosomal granules in round spermatids. Stages IV-V were defined by the presence of two generations of spermatids, and round spermatids with caps or flattened granules. Stages VI-VIII were defined by two generations of spermatids with round spermatids exhibiting acrosomes covering one- to two-thirds of the round spermatid. Stage IX was characterized as the time point at which round spermatids of Stage VIII begin to elongate and to lose their round character, with only one generation of spermatids present. Stage X was characterized by elongating spermatids becoming bilaterally flattened, with only one generation of spermatids present. Stage XI was characterized by one generation of elongated spermatids, by the presence of diplotene/zygotene spermatocytes, and by the lack of meiotic events. Stage XII was characterized by one generation of elongated spermatids and the presence of meiotic events.

Meiotic tubule, spermatocyte, and spermatid quantification

H3f3b null (n = 5) and WT (n = 4) testis were stained with H3 S10P antibody (Millipore 06-570, 1:200) and LectinPNA (Invitrogen L21409, 1:100) to quantify the number of meiotic tubules per testis slice (see Table S8). For each testis section (n = 15 WT and n = 18 null) the total number of tubules was counted. Meiotic (Stage XII) tubules were defined strictly by the presence of H3pS10^{+} cells within the tubule lumen. To determine the number of H3 S10P^{+} cells per tubule area, seminiferous tubule area and the number of H3 S10P^{+} cells were determined using ImageJ software from n = 51 null and n = 43 WT Stage XII tubules. For round spermatid analysis, n = 5 null and n = 4 WT mouse testes samples were quantified in a total of n = 8 null and n = 7 testes sections (see Table S8). LectinPNA staining was used to locate Stage I tubules; n = 62 *H3f3b* WT and n = 48 *H3f3b* null Stage I tubules analyzed. Stage I tubules were quantified for round (step 1) and elongated (step 13) spermatids using ImageJ software (http://rsb.info.nih.gov/ij/) based on cell size and shape factor.

CENP-A foci analysis

CENP-A foci quantification was performed as described in (Bush et al., 2013). A total of n = 6 WT and n = 8 null confocal Z-stack images (an average of 20 sections per image) were analyzed using ImageJ software for CENP-A^{+} foci. Spermatogonia and spermatocyte cell regions of interest were selected along or 1-2 cell layers luminally from the tunica propria of the seminiferous tubule (n = 555 null and n = 217 WT cells) from null #13 and WT #14 testes.

Sperm assessment and staining

Male animals (n = 5 null, n = 3 WT) were submitted to the UC Davis Mouse Biology Program for sperm analysis. Sperm were isolated from animals using the swim-out method from the epididymis in conjunction with the UC Davis Mouse Biology Program. For sperm motility, 10 µL sperm was mixed with 190 µL of warm M2 medium, and the sperm concentration, total motility (% motile sperm), rapid sperm motility (% of motile sperm with VAP ≥ 10 µm/sec), and progressive motility (% of motile sperm with VAP ≥ 50 µm/sec and STR ≥ 50%) were assessed using an IVOS computerized sperm analyzer (Hamilton Thorne) at 37°C. VAP: average cell path velocity in µm/sec; VSL: the straight line velocity in µm/sec; STR: the straightness ratio of VSL/VAP, expressed as a percent. At least 1,000 sperm were analyzed per male mouse. Sperm morphology was assessed under a phase-contrast microscope, and at

least 100 sperm were scored for percentages of abnormal sperm heads (triangular, olive, pin, banana, amorphous, collapsed, and abnormal hook) and sperm tails (bent, coiled, crinkled). For staining, approximately 5 x 10^6 spermatozoa were plated out per slide. Slides were air-dried and frozen at -80°C and thawed prior to use. Decondensation of spermatozoa was performed using 200 µL of 0.01 M DTT, 0.1 U heparin (MP Biomedicals #194110, 10 U/µL), and 0.2% Triton X-100 for 45 min at RT. Slides were then air-dried for 10 min, and then immediately fixed in 100% ice-cold methanol for 10 min. Slides were then air dried for 10 min, washed once in 1X PBS for 5 min, and then blocked in 10% normal goat serum in TBS for 30 min. Slides were then washed 1X in PBS for 5 min, and then 200 µL of primary antibody diluted in carrier solution (1% BSA in TBS) was applied and incubated overnight at 4°C. The next day, 0.025% Triton X-100 in TBS was used to wash the slides, 2X for 5 min each. 200 µL secondary antibody in carrier solution was applied and incubated for 105 min at RT. Slides were washed 2X in 0.025% Triton X-100 in TBS, and once in TBS for 5 min each. Slides were then mounted using Vectashield mounting medium with DAPI (Vector Labs #H1200) and imaged under a Biorevo BZ-9000 microscope system (Keyence).

TUNEL staining and quantification

Paraffin-embedded testes sections from n = 6 null and n = 4 WT males, or spermatozoa slides from n = 2 WT and n = 3 null males (refer to Table S8) were used for TUNEL staining (DeadEnd Fluorometric TUNEL System, Promega G3250). $TUNEL^+$ tubules were scored (n = 3 null and WT) as the number of seminiferous tubules exhibiting one or more apoptotic events out of the total number of tubules per testis. Scoring was also done by another blinded researcher. Quantification of apoptotic nuclei was performed using ImageJ software, scoring $TUNEL^+$ nuclei out of the total $DAPI^+$ nuclei per image.

Ahmed, E. A. and de Rooij, D. G. (2009). Staging of mouse seminiferous tubule cross-sections. *Methods Mol Biol* **558**, 263-77.
Bush, K. M., Yuen, B. T., Barrilleaux, B. L., Riggs, J. W., O'Geen, H., Cotterman, R. F. and Knoepfler, P. S. (2013). Endogenous mammalian histone H3.3 exhibits chromatin-related functions during development. *Epigenetics Chromatin* **6**, 7.
Carvalho, B. S. and Irizarry, R. A. (2010). A framework for oligonucleotide microarray preprocessing. *Bioinformatics* **26**, 2363-7.
Gardiner-Garden, M. and Frommer, M. (1987). CpG islands in vertebrate genomes. *J Mol Biol* **196**, 261-82.
Gaucher, J., Boussouar, F., Montellier, E., Curtet, S., Buchou, T., Bertrand, S., Hery, P., Jounier, S., Depaux, A., Vitte, A. L. et al. (2012). Bromodomain-dependent stage-specific male genome programming by Brdt. *EMBO J* **31**, 3809-20.

Gaysinskaya, V., Soh, I. Y., van der Heijden, G. W. and Bortvin, A. (2014). Optimized flow cytometry isolation of murine spermatocytes. *Cytometry A*.
Gentleman, R. C., Carey, V. J., Bates, D. M., Bolstad, B., Dettling, M., Dudoit, S., Ellis, B., Gautier, L., Ge, Y., Gentry, J. et al. (2004). Bioconductor: open software development for computational biology and bioinformatics. *Genome Biol* **5**, R80.
Getun, I. V., Torres, B. and Bois, P. R. (2011). Flow cytometry purification of mouse meiotic cells. *J Vis Exp*.
Heinz, S., Benner, C., Spann, N., Bertolino, E., Lin, Y. C., Laslo, P., Cheng, J. X., Murre, C., Singh, H. and Glass, C. K. (2010). Simple combinations of lineage-determining transcription factors prime cis-regulatory elements required for macrophage and B cell identities. *Molecular cell* **38**, 576-89.
Hess, R. A. and Renato de Franca, L. (2008). Spermatogenesis and cycle of the seminiferous epithelium. *Adv Exp Med Biol* **636**, 1-15.
Kent, W. J., Sugnet, C. W., Furey, T. S., Roskin, K. M., Pringle, T. H., Zahler, A. M. and Haussler, D. (2002). The human genome browser at UCSC. *Genome Res* **12**, 996-1006.
Langmead, B., Trapnell, C., Pop, M. and Salzberg, S. L. (2009). Ultrafast and memory-efficient alignment of short DNA sequences to the human genome. *Genome Biology* **10**, R25.
Meistrich, M. L. and Hess, R. A. (2013). Assessment of spermatogenesis through staging of seminiferous tubules. *Methods Mol Biol* **927**, 299-307.
Mohn, F., Weber, M., Rebhan, M., Roloff, T. C., Richter, J., Stadler, M. B., Bibel, M. and Schubeler, D. (2008). Lineage-specific polycomb targets and de novo DNA methylation define restriction and potential of neuronal progenitors. *Mol Cell* **30**, 755-66.
Ross-Innes, C. S., Stark, R., Teschendorff, A. E., Holmes, K. A., Ali, H. R., Dunning, M. J., Brown, G. D., Gojis, O., Ellis, I. O., Green, A. R. et al. (2012). Differential oestrogen receptor binding is associated with clinical outcome in breast cancer. *Nature* **481**, 389-93.
Tan, M., Luo, H., Lee, S., Jin, F., Yang, J. S., Montellier, E., Buchou, T., Cheng, Z., Rousseaux, S., Rajagopal, N. et al. (2011). Identification of 67 histone marks and histone lysine crotonylation as a new type of histone modification. *Cell* **146**, 1016-28.

Supplemental Figure Legends.

Supplemental Figure 1. Expression of H3.3 greatly reduced in *H3f3b* null testes. (A). Loss of *H3f3b* did not have a significant impact on total H3 protein present in the testes, normalized to β-actin. (B). The ratio of H3 to β-actin within WTCL was not significantly different between null and WT testes. (C). Null testes displayed significantly lower levels of H3.3 protein by Western blot, including significant reductions in higher molecular-weight H3.3 bands. (D). A separate set of null testes also displayed significantly lower levels of H3.3 protein by Western blot. (E). H3.3 levels were found to be significantly decreased in null samples compared to WT (p = 0.005). (F). Comparison of H3.3 expression (red) in Stage II-III tubules between null and WT testes. H3.3 is strongly expressed at Stage II-III in WT spermatogonia cells, round spermatids, and pachytene spermatocytes. H3.3 is also expressed in bright focal points within the nuclear interior of round spermatids in WT (protein bodies, white arrows) and displays weak focal expression in WT pachytene spermatocytes (white arrowheads) at this stage. H3.3 was nearly undetectable in null spermatogonia cells and was only weakly expressed in null round spermatids (faint focal points) and in few pachyene spermatocytes (diffuse nuclear staining). Higher magnification is displayed in lower right hand corner of the pictured seminiferous tubule. (G). Comparison of H3.3 expression between Stage IV-V tubules in WT and null testes. H3.3 is strongly expressed in WT spermatogonia, pachytene spermatocytes, and round spermatids at Stage IV-V. In contrast, H3.3 expression became faintly detectable in spermatogonia and pachytene spermatocytes (white arrowheads) in null tubules. Null tubules also exhibited slight increases in H3.3 expression in round spermatids (white arrows), although significantly lower than in WT. DAPI (blue) was used for counterstaining. Higher magnification is displayed in lower right hand corner of the pictured seminiferous tubule. White dotted lines indicate borders of specified tubule. Scale bars = 100 μm.

Supplemental Figure 2. Localization and levels of H3.3, H3K9me3, TUNEL, Tnp1, and Prm1 during spermatogenesis. (A). WT spermatogonia display weak expression of H3.3 and H3K9me3, with only intermittent apoptotic events. WT spermatocytes begin to exhibit elevated H3K9me3 levels during zygotene and early pachytene, and H3K9me3 levels begin to decrease corresponding to the expression of H3.3 in early pachytene. TUNEL^{+} events appear to coincide with changes in H3K9me3 levels during leptotene and zygotene and late pachytene. In WT, H3.3 levels begin to decrease in late-stage spermatids (step 10-11), corresponding to increased expression of Tnp1 and Prm1. (B). Null spermatogonia display very low or undetectable H3.3 expression, and H3K9me3 levels begin to increase in intermediate (Int)-type spermatogonia and persist through the leptotene transition. Significantly more apoptotic events are also present in spermatogonia compared to WT. In null spermatocytes, elevated H3K9me3 levels persist to mid-pachytene and begin to decrease during late pacyhtene, though still remain higher than WT. The decrease in H3K9me3 in null tubules corresponds to the weak expression of H3.3 that occurs in mid-pachytene spermatocytes. Apoptotic events (TUNEL^{+}) correspond to WT-timed apoptotic events, though are present at higher levels and in a broader range of cell types and stages. In null spermatids, H3.3 levels begin to decrease in later-stage spermatids (step 10-11) as in WT, although H3.3 levels are already significantly lower than in WT. H3K9me3 levels also appear to persist longer in nulls than in WT in late-stage spermatids. Corresponding to the earlier decrease in H3.3 levels in the null, Tnp1 and Prm1 expression begin earlier in null tubules (Stage IX-X) than in WT, although Prm1 levels are significantly lower than in WT. Abbreviations: A (A-type spermatogonia), Int (intermediate-type spermatogonia), B (B-type spermatogonia), pL (pre-leptotene spermatocyte), L9-L10 (leptotene spermatocytes found in Stage IX-X), Z11-Z12 (zygotene spermatocytes found in Stage XI-XII), P1-10 (pachytene spermatocytes found in Stage I-X), D (diplotene spermatocytes), M (meiotically-dividing spermatocytes), 1-16 (spermatids in steps 1-16 of development).

Supplemental Figure 3. Gross defects in *H3f3b* null testes. (A). Testes size was significantly reduced in null males. Other organs (heart, right) did not display differences in mass or size between null and WT. (B). WT and null animals did not display significant differences in body mass or size. (C-D). Null males displayed significantly lower testes mass (C), even when normalized to animal weight (D). (E). *H3f3b* null testes do not present a significantly reduced number of seminiferous tubules when compared to WT. (F). Hematoxylin and eosin (H&E) staining of null and WT testes sections. (Upper panels) Null tubules typically exhibit an open lumen when compared to WT (scale bars = 500 μm). (Lower panels) Early- to mid-stage null seminiferous tubules (scale bars = 100 μm) display altered architecture and a decreased number of spermatids. (G-I). Null tubules display significantly reduced counts of total spermatids (G) when normalized to seminiferous tubule area, and a significantly lower average number of round (H) and elongated (I) spermatids in Stage I tubules when normalized to tubule area.

Supplemental Figure 4. FACS analysis and sorting methodology. FACS sorting was performed according to previously published studies (Bastos et al., 2005; Gaysinskaya et al., 2014; Getun et al., 2011), with minor modifications (see Supplemental Methods). (A). Initial FACS gating was performed on the entire population of Hoechst33342^{+} cells. Hoechst Blue is shown on the Y-axis and Hoechst Red is shown on the X-axis. The representative image depicted here is of male WT #4198. (B). Further gating was performed to eliminate dead cells. At the time of the sort, propidium iodide (PI) was added to exclude dead (PI^{+}) cells. Hoechst 33342^{+}, PI^{-} cells were gated for further analysis. Side scatter (SSC) is shown on the Y-axis, PI is shown on the X-axis. (C). Size exclusion. Our gating methodology selected for cells with standard shape and size within the testes and to exclude debris. SSC is shown on the Y-axis, forward scatter (FSC) is shown on the X-axis. (D). Population gating of spermatogonia (Spg, yellow), pre-leptotene spermatocytes (pL-Spc, blue), spermatocytes (Spc, red), and spermatids (Sptd, purple) for WT #4198. Hoechst Blue is shown on the X-axis, Hoechst Red is shown on the Y-axis. (E). Gated

populations of Spg, pL-Spc, and Spc separate out into distinct populations as previously described in (Bastos et al., 2005; Gaysinskaya et al., 2014). SSC is shown on the Y-axis, FSC is shown on the X-axis. (F). Individual populations of Spg, pL-Spc, Spc, and Sptd separate out into distinct populations based on size and complexity. SSC is shown on the Y-axis, FSC is shown on the X-axis. (G). Enrichment analysis on sorted cells. Cells placed onto coverslips were examined for size and acrosomal expression by lectinPNA staining (upper left). Sptd populations were found to have significant enrichment for small, acrosome^{+} cells. The Sptd population was also found to have high enrichment of *Prm1* expression (lower left), specifically expressed in Sptd populations normally (Campbell et al., 2013). Finally, the Spc population was found to have substantially higher enrichment for synaptonemal complex protein 3 (Sycp3, upper right), a marker predominantly expressed in spermatocytes with some expression in pre-leptotene spermatocytes (Gaysinskaya et al., 2014). (H). Representative images of Spg, pL-Spc, Spc, and Sptd populations. Scale bars = 20 μm.

Supplemental Figure 5. FACS analysis on *H3f3b* null testes. (A). Pseudocolor gating of WT #4263 cells according to the FACS methodology described in Figure S4. Spermatogonia (Spg, red), pre-leptotene spermatocytes (pL-Spc, blue), spermatocytes (Spc, red), and spermatid (Sptd, purple) gates are shown. (B). Pseudocolor gating of Null #4240. Hoechst Blue is shown on the Y-axis, Hoechst Red is shown on the X-axis. (C-F). Analysis of combined populations of WT #4198, 4263 vs. Null #4176, 4240-4242. (C). *H3f3b* WT and null testes did not significantly differ in the proportion of spermatogonia (10.85% WT vs. 9.51% null, p = 0.195). (D). WT and null testes did not differ significantly in the proportion of spermatocytes present (7.78% WT vs. 10.51% null, p = 0.239). (E). Null testes exhibited a slight but significant increase in the proportion of spermatids present (6.11% WT vs. 7.6% null, p = 0.033). (F). Null testes displayed significant reductions in the amount of pre-leptotene spermatocytes present (9.37% WT vs. 4.91% null, p = 0.020).

Supplemental Figure 6. Null testes do not exhibit significant increases in meiotic markers or in Cenpa expression. (A). Stage XII meiotic tubules were identified by the presence of H3 S10P^{+} spermatocytes in the tubule lumen of late-stage seminiferous tubules with one generation of spermatids present. *H3f3b* testes do not exhibit significantly higher numbers of meiotic tubules when normalized to total number of tubules present per testis. (B). Null tubules do not display a higher percentage of H3 S10P^{+} cells per tubule area compared to WT. (C). The number of Cenpa^{+} foci per spermatocyte or spermatogonia cell was not significantly different between WT or null animals. (D). Analysis of Cenpa^{+} foci in WT and null spermatocytes and spermatogonia did not reveal significant differences in the percent of Cenpa^{+} foci when normalized to cell area.

Supplemental Figure 7. Apoptotic events primarily found around late-stage seminiferous tubules of *H3f3b* null testes. (A). When compared to stage-matched *H3f3b* WT tubules, a large proportion of apoptotic events were detected in null Stage IX tubules. White arrows indicate leptotene or pachytene spermatocytes, white arrowheads indicate spermatogonia. (B). Stage X tubules exhibited apoptotic events less frequently than Stage IX in null tubules, and apoptotic nuclei were generally smaller in size, possibly indicating nuclear breakdown following apoptosis. White arrows indicate apoptotic pachytene or leptotene spermatocytes. (C). Comparison of apoptotic events during late-stage tubules. TUNEL^{+} nuclei were primarily detected around Stage IX, with decreasing amount of apoptotic nuclei detected in subsequent stages of spermatogenesis (Stage X, XI, XII). (D). A separate testis with the majority of apoptotic nuclei appearing in late-stage tubules, and the bulk of events taking place around Stage IX. DAPI (blue) was used for counterstaining. White dotted lines indicate borders of specified tubule. Scale bars = 100 μm.

Supplemental Figure 8. Disruption of normal H3K9me3 levels in *H3f3b* null tubules. (A). Levels of the H3K9me3 heterochromatic mark were increased in null testes. Scale bars = 500μm. (B). Whole testes cell lysate (WTCL) revealed that H3K9me3 levels were only modestly increased on a global level when normalized to β-actin. (C). H3K9me3 levels in a separate age-matched set of littermates revealed only moderate increases in H3K9me3 globally when normalized to β-actin. (D). Quantification of H3K9me3 levels in WTCL did not present a significant increase of H3K9me3 in nulls when compared to WT and normalized to β-actin. Bars represent the averages of 5 nulls normalized to WT. (E). Sorted pre-leptotene spermatocytes stained for H3K9me3 (green). Null pre-leptotene spermatocytes have substantially higher amounts of H3K9me3 by IHC-IF when compared to WT. DAPI (blue) was used for counterstaining. Scale bars = 20 μm. (F). Sorted null pre-leptotene spermatocytes (pL-Spc) displayed a significant 1.97-fold increase in H3K9me3 (p = 2.29 x 10^{-12}; n = 518 WT and 408 null cells analyzed). (G). Null spermatocytes (Spc) sorted by FACS exhibited slight but non-significant increases in H3K9me3 (p = 0.329; n = 268 WT and 689 null cells analyzed). (H). Null spermatocytes positive for γH2A.X exhibited slight increases in H3K9me3 when compared to WT γH2A.X^+ Spc, but the level of significance was even less than that between WT and null Spcs (p = 0.584; n = 78 WT and 48 null cells analyzed).

Supplemental Figure 9. *H3f3b* loss produces increases in H3K9me3 levels. (A). H3K9me3 levels were generally increased in *H3f3b* null tubules. Stage IX tubules, exhibiting a majority of spermatids beginning to undergo elongation, demonstrated elevated H3K9me3 levels in spermatogonia, leptotene spermatocytes, and spermatids, with increased diffuse staining of pachytene spermatocytes. (B). Null Stage X tubules exhibiting bilaterally flattening spermatids displayed elevated H3K9me3 levels in spermatogonia, leptotene spermatocytes, and elongating spermatids along with elevated H3K9me3 in pachytene spermatocytes. (C). Stage XII tubules displayed elevated H3K9me3 in meiotic and secondary spermatocytes with strongest staining in

zygotene spermatocytes and spermatogonia. H3K9me3 is shown in green, DAPI (blue) was used for counterstaining. Scale bars = 10 μm.

Supplemental Figure 10. Increased H3K9me3 expression in *H3f3b* null germ cells relative to H3K4me2/me3. *H3f3b* WT and null testes were stained for H3K9me3 and di- and trimethylation of K4 on H3 (H3K4me2/me3). H3K9me3 is shown in green, H3K4me2/me3 is shown in red, and DAPI (blue) was used for counterstaining. Relative to H3K4me2/me3, H3K9me3 levels were higher in *H3f3b* null germ cell types as shown in mid-stage (spermatogonia, spermatocytes, and round spermatids), Stage XI (spermatogonia, spermatocytes, and elongating spermatids), and Stage XII (spermatogonia, spermatocytes, secondary spermatocytes, and elongated spermatids). Scale bars = 20 μm.

Supplemental Figure 11. H3K4me3, H3K27me3, and H3.3 S31P PTM levels in *H3f3b* null and WT testes. (A). The euchromatic H3K4me3 post-translational histone modification was decreased overall in *H3f3b* null testes compared to WT. The majority of strong H3K4me3 signal emanated from the layer of cells closest to the tunica propria in tubules, corresponding to regions of spermatogonia or spermatocytes in null and WT testes. Scale bars = 500μm. (B). Levels of H3K4me3 were moderately decreased overall in nulls when compared to age-matched WT littermates by WTCL. (C). Quantification of H3K4me3 levels from WTCL did not show a significant decrease in H3K4me3 levels when compared to WT. Bars represent the averages of 5 nulls and 2 WTs. (D). Two separate sets of WTCL from age-matched littermates were probed for H3K27me3 and H3.3 S31P. *H3f3b* null testes did not display significantly elevated levels of H3K27me3, but did exhibit drastic increases in H3.3 S31P relative to the total amount of H3.3 protein present (compare to H3.3 levels, Fig. S1C,D). (E). H3.3 S31P (red) localized primarily to meiotically dividing spermatocytes in Stage XII tubules in both WT and null

animals. DAPI (blue) was used for counterstaining. White dotted lines indicate borders of specified tubule. Scale bars = 100μm.

Supplemental Figure 12. ChIP-seq data overlap and H3K4me3 peak analysis. (A). The *H3f3b* locus contains no reads mapping to the exons 2-4 affected by the null, validating the genotype. (B). Analysis of HOMER-called consensus peak widths for testes H3K4me3 indicates that null samples display significantly less peaks than WT ($p < 2 \times 10^{-16}$, Turkey's Honestly Significant Difference Test), with WT peaks being larger. (C-D). Overlap of peaks in WT (C) and null (D) ChIP-seq samples.

Supplemental Figure 13. Clustering and satellite analysis of *H3f3b* WT and null ChIP-seq samples and qPCR for genes up- or down-regulated by microarray and ChIP-seq. (A). DiffBind clustering of WT and null ChIP-seq peaks indicates that the two WT samples are highly similar to each other, while the two null samples are more divergent. Both WT and both null samples cluster together, suggesting reproducible differences in the distribution of H3K4me3 caused by the knockout. (B). H3K4me3 tag counts mapping to major and minor satellite repeats, normalized by the number of reads mapping to the matched input controls, show no clear difference between WT and null samples. (C-H). Data presented are the average fold-change of n = 2 testes RNA samples for each null over WT. Error bars indicate standard deviations. (C-E). Fold-change of (C) *Snai1,* (D) *Gpt2*, and (E) *Prkra* found to be up-regulated by microarray with gained H3K4me3 peaks by ChIP-seq in null testes. (F-H). Fold change of (F) *Lrrc52*, (G) *Catsper3*, and (H) *Hk1* found to be down-regulated by microarray with lost H3K4me3 peaks by ChIP-seq in null testes.

Supplemental Figure 14. Overlap of *H3f3b* null genes up- and downregulated by microarray to genes identified in H3K4me3 ChIP-seq datasets. Genes up- or downregulated by a factor of

1.5-fold by microarray were found to overlap significantly with their respective ChIP-seq datasets. (A-B). A significant proportion of genes downregulated by 1.5-fold or greater by microarray overlapped with genes found to have (A) decreased H3K4me3 peaks (p = 5.49 x 10^{-12}) or with (B) genes which lost H3K4me3 peaks (p = 1.34 x 10^{-32}) by ChIP-seq. (C-D). In addition, genes upregulated by 1.5-fold or greater by microarray overlapped with genes (C) found to have increased H3K4me3 peaks (p = 0.043) and with (D) genes found to have unique H3K4me3 peaks by ChIP-seq (p = 0.030).

Supplemental Figure 15. Loss of H3K4me3 peaks around *Tnp1* in *H3f3b* null males and analysis of *Prm1-3* and *Tnp1-2* in sorted spermatid populations. (A). Null samples display overall reduced H3K4me3 ChIP-seq peaks with a specific loss of H3K4me3 peaks around the transition protein 1 gene, *Tnp1*. (B). Null and WT whole testes RNA does not reveal a significant difference in *Tnp1* expression (p = 0.227). (C-I). qPCR expression analysis for *Prm1-3* and *Tnp1-2* on spermatid populations sorted by FACS (WT #4198, 4263 vs. Null #4176, 4240-4242). (C). Overall expression of *Prm1* between combined WT and null samples does not reveal a significant difference in expression (p = 0.169). (D). Overall expression of *Prm2* between combined WT and null spermatid populations does not reveal a significant difference in expression (p = 0.054). (E). Though *Prm1* expression was not significantly different between WT and null samples when combined, individual analysis of *Prm1* expression between each spermatid population revealed that one null sample (Null #4240) exhibited abnormally high *Prm1* transcript levels. The remainder of the null samples (Null #4176 vs. WT #4198; Null #4241-4242 vs. WT #4263) exhibited substantially lower *Prm1* transcript levels. (F). *Prm2* expression was not significantly different between WT and null samples when combined, though individual analysis of *Prm2* expression between spermatid populations again revealed that one null sample (Null #4240) exhibited abnormally high *Prm2* transcript levels relative to other null samples. Null samples #4176, 4241, and 4242 all displayed substantially lower levels of *Prm2*

transcript relative to their age-matched WT control. (G). Combined null samples exhibit significant overall decreases in *Prm3* expression relative to combined WT samples (p = 0.032). (H). Combined null samples exhibit significant overall decreases in *Tnp2* expression relative to combined WT samples (p = 3.32 x 10^{-6}). (I). There was not a significant difference between combined null and WT samples in overall *Tnp1* expression (p = 0.222).

Supplemental Figure 16. Loss of *H3f3b* perturbs normal protamine incorporation and induces significant increases in H3K9me3 and apoptosis in sperm. (A). Under normal conditions, Prm1 (red) is strongly expressed in mid-stage seminiferous tubules, corresponding to step 15-16 spermatids. In null males, Prm1 expression was significantly reduced in mid-stage seminiferous tubules when compared to WT. Although some Prm1 incorporation is evident in null tubules, Prm1 expression was overall reduced in null animals analyzed. DAPI (blue) was used for counterstaining. White dotted lines indicate borders of specified tubule. Scale bars = 100 μm. (B). Stage XII WT and null meiotic tubules were used to quantify the proportion of $Prm1^+$ step 12 spermatids. 31.6% of WT spermatids were found to be $Prm1^+$ compared to a significantly smaller proportion of null spermatids at this stage (10.7%, p = 0.038). (C). Decondensed null sperm exhibited remarkably higher proportions of $H3K9me3^+$ (red) sperm and of apoptotic ($TUNEL^+$, green) sperm when compared to WT. DAPI (blue) was used for counterstaining. Scale bars = 20 μm. (D). Approximately 58.5% of null sperm were also positive for H3K9me3, while only 16.6% of WT sperm were positive for H3K9me3 (p = 8.38 x 10^{-12}). (E). Large proportions of decondensed null sperm (23.2%) were found to be apoptotic, compared to only 1.9% of decondensed WT sperm (p = 2.48 x 10^{-23}). (F). Decondensed null sperm that were positive for H3K9me3 were also found to be highly apoptotic (18.8% of $H3K9me3^+$ sperm were also $TUNEL^+$) when compared to WT (1.7%, p = 4.73 x 10^{-9}).

Supplemental Movie 1. WT sperm morphology and movement. WT sperm are phenotypically normal and do not display severe defects in movement. The majority of sperm is motile and is capable of producing progressive forward movement.

Supplemental Movie 2. *H3f3b* null sperm morphology and movement. The vast majority of null sperm is phenotypically abnormal and exhibit severe defects in movement. Most sperm are not motile and capable of producing progressive forward movement.

Bastos, H., Lassalle, B., Chicheportiche, A., Riou, L., Testart, J., Allemand, I. and Fouchet, P. (2005). Flow cytometric characterization of viable meiotic and postmeiotic cells by Hoechst 33342 in mouse spermatogenesis. *Cytometry A* **65**, 40-9.
Campbell, P., Good, J. M. and Nachman, M. W. (2013). Meiotic sex chromosome inactivation is disrupted in sterile hybrid male house mice. *Genetics* **193**, 819-28.
Gaysinskaya, V., Soh, I. Y., van der Heijden, G. W. and Bortvin, A. (2014). Optimized flow cytometry isolation of murine spermatocytes. *Cytometry A*.
Getun, I. V., Torres, B. and Bois, P. R. (2011). Flow cytometry purification of mouse meiotic cells. *J Vis Exp*.

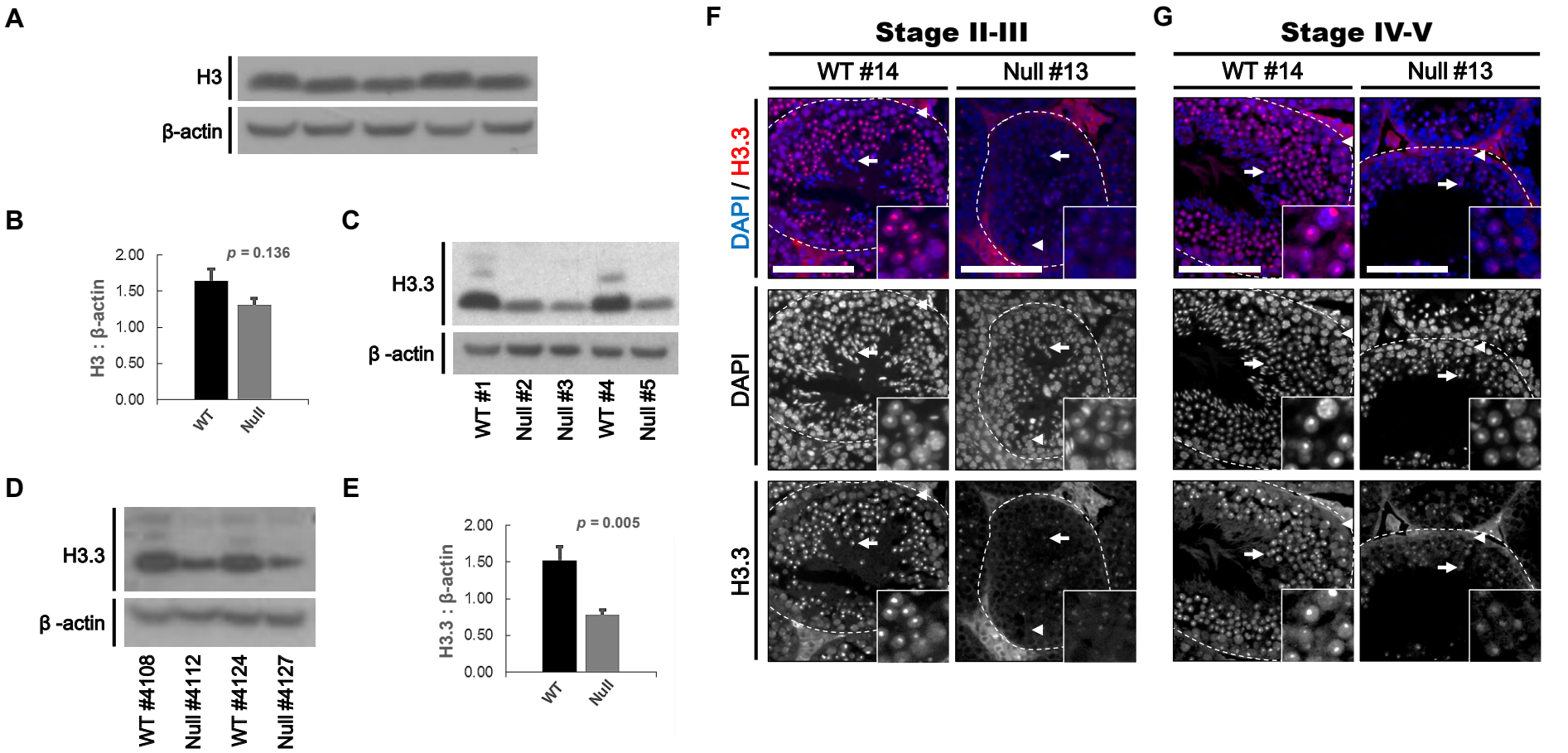

Yuen et al., Supplemental Figure 1

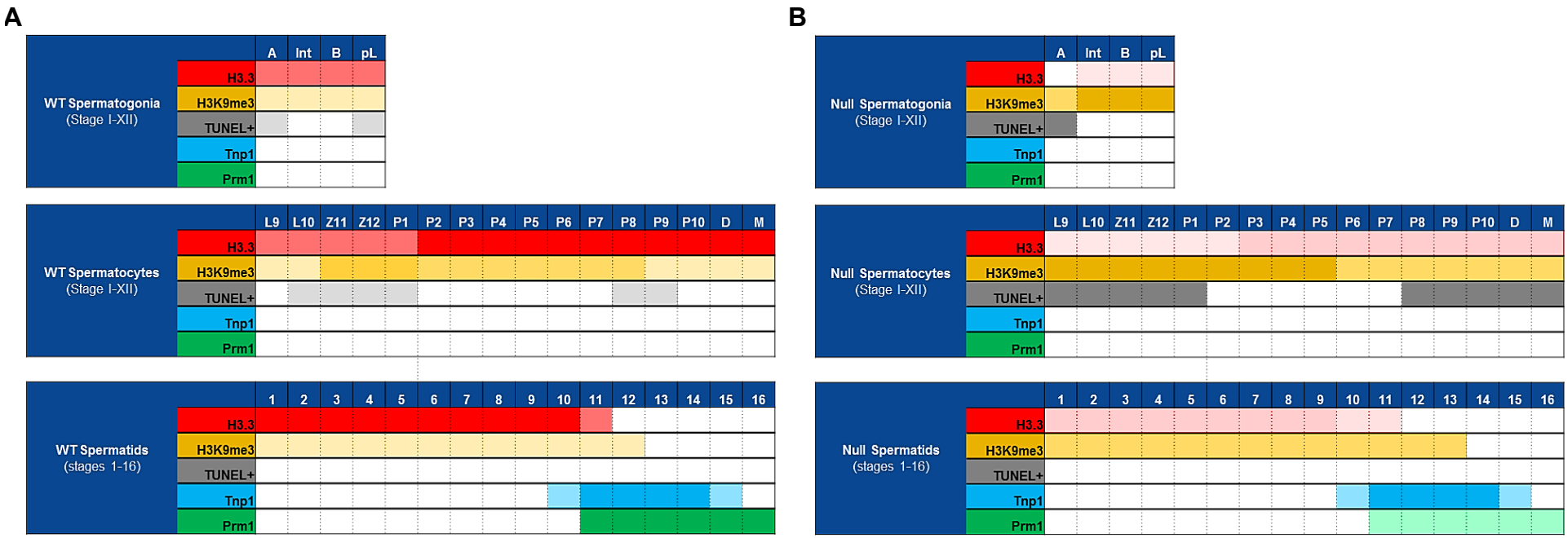

Yuen et al., Supplemental Figure 2

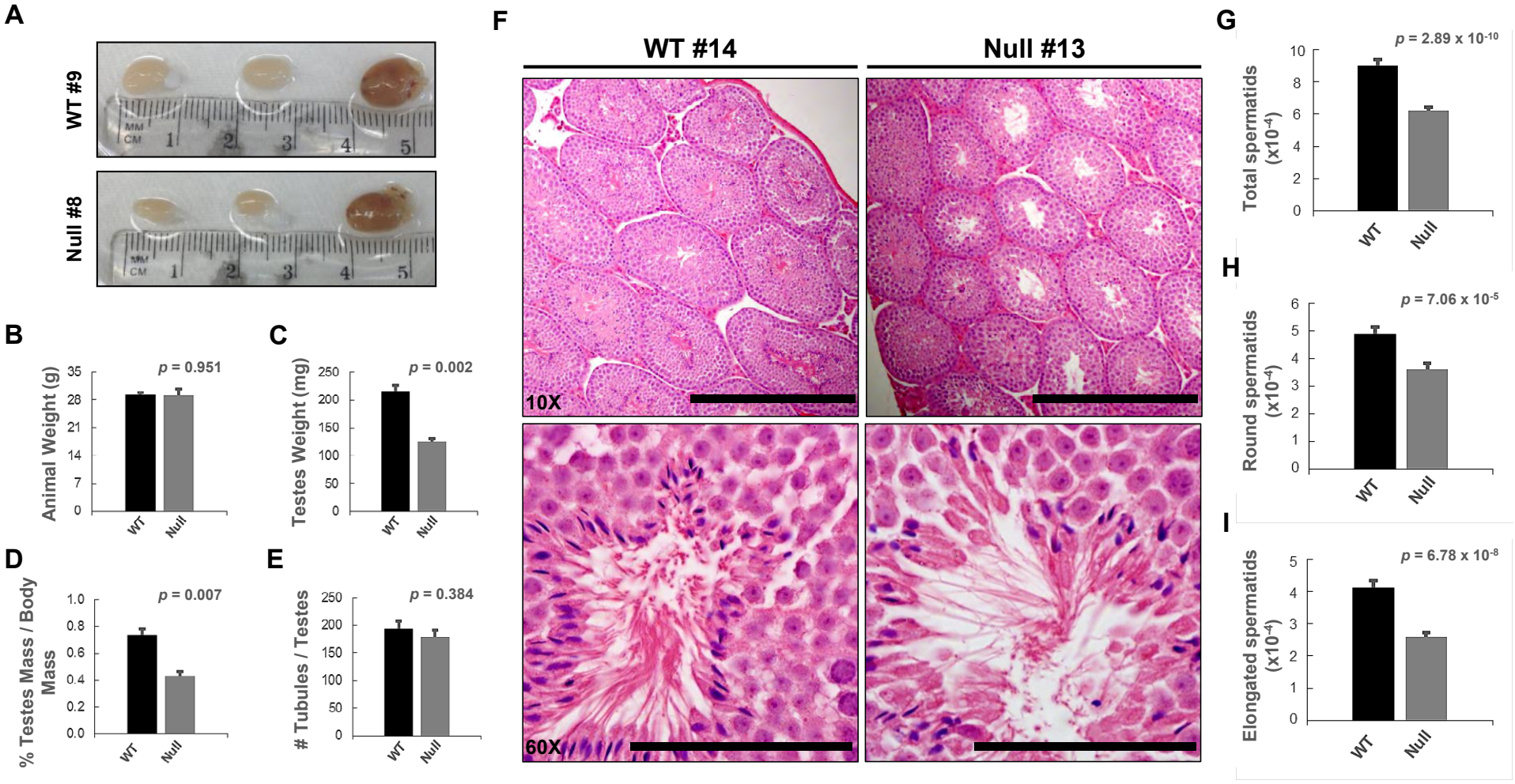

Yuen et al., Supplemental Figure 3

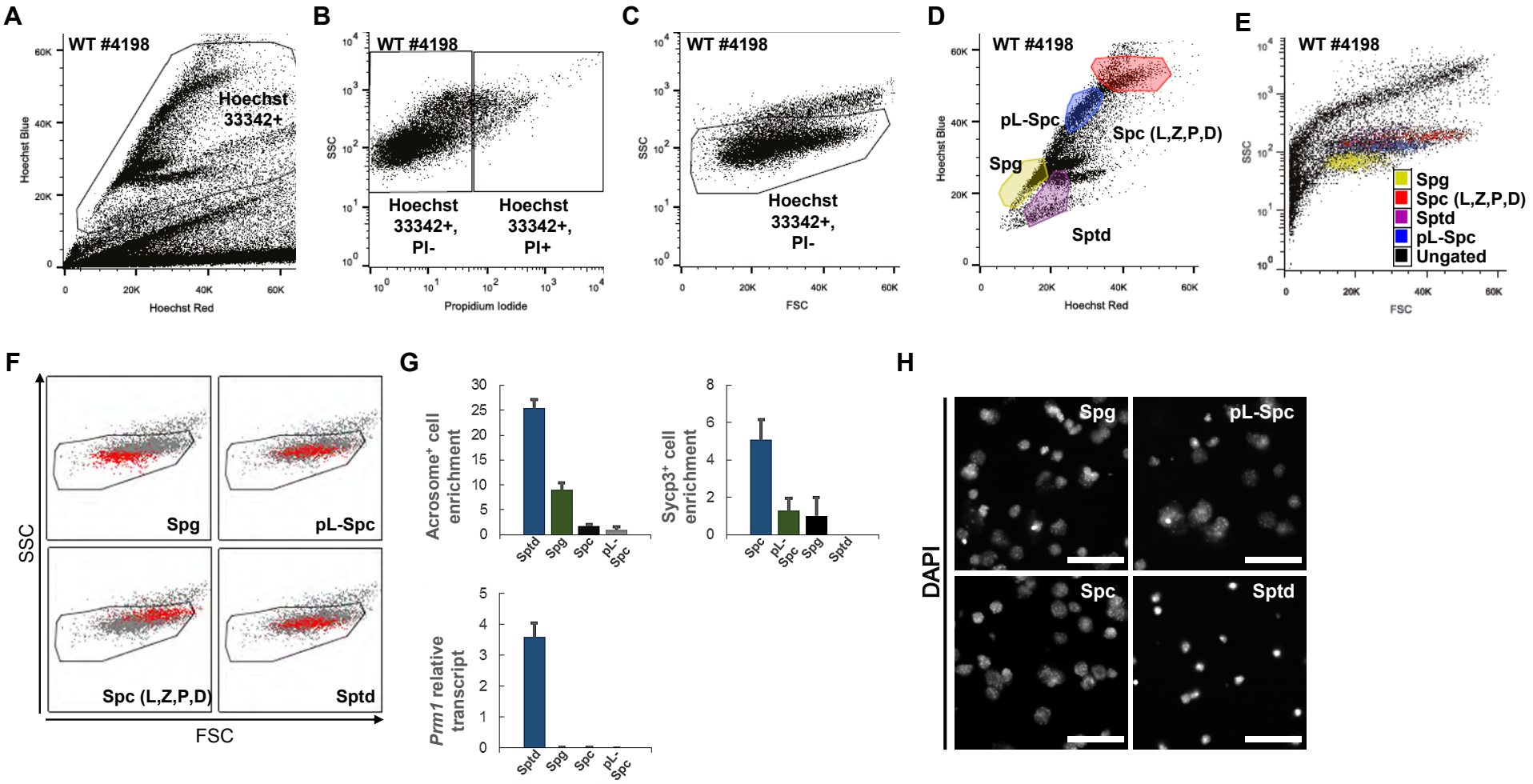

Yuen et al., Supplemental Figure 4

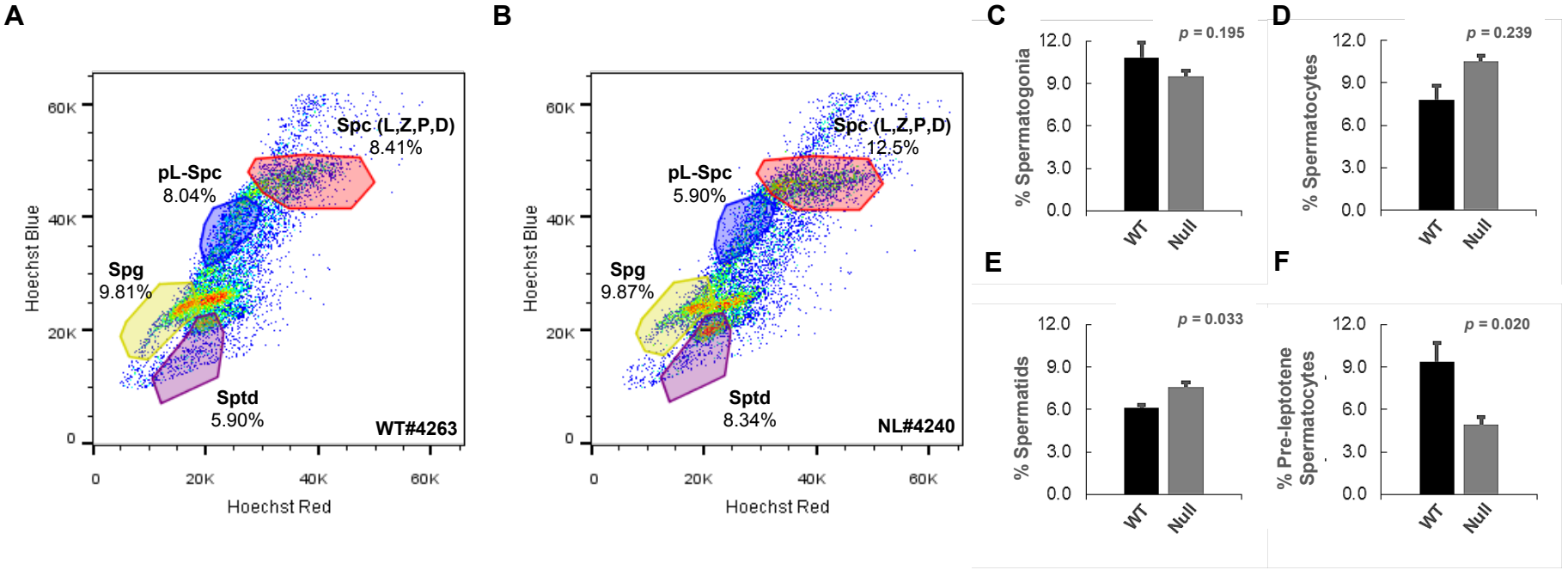

Yuen et al., Supplemental Figure 5

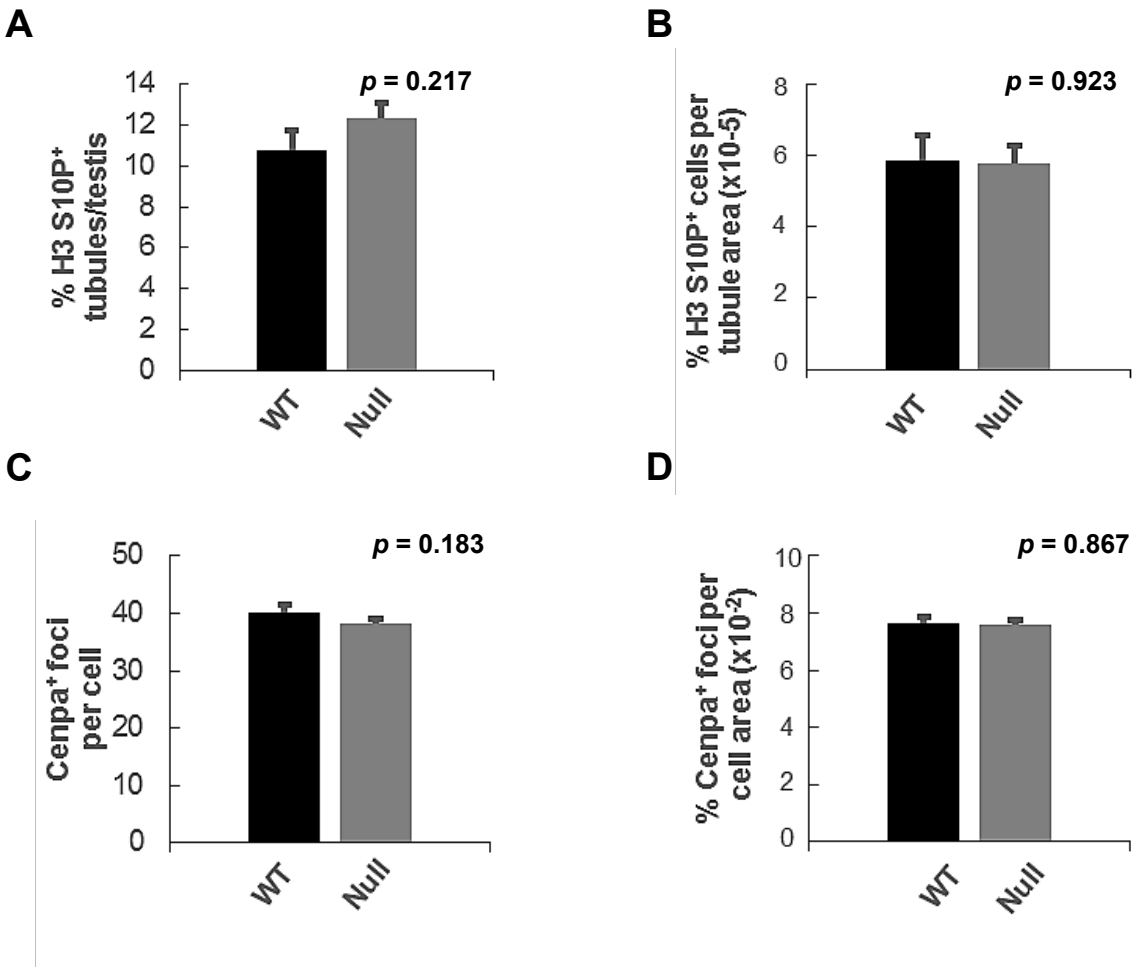

Yuen et al., Supplemental Figure 6

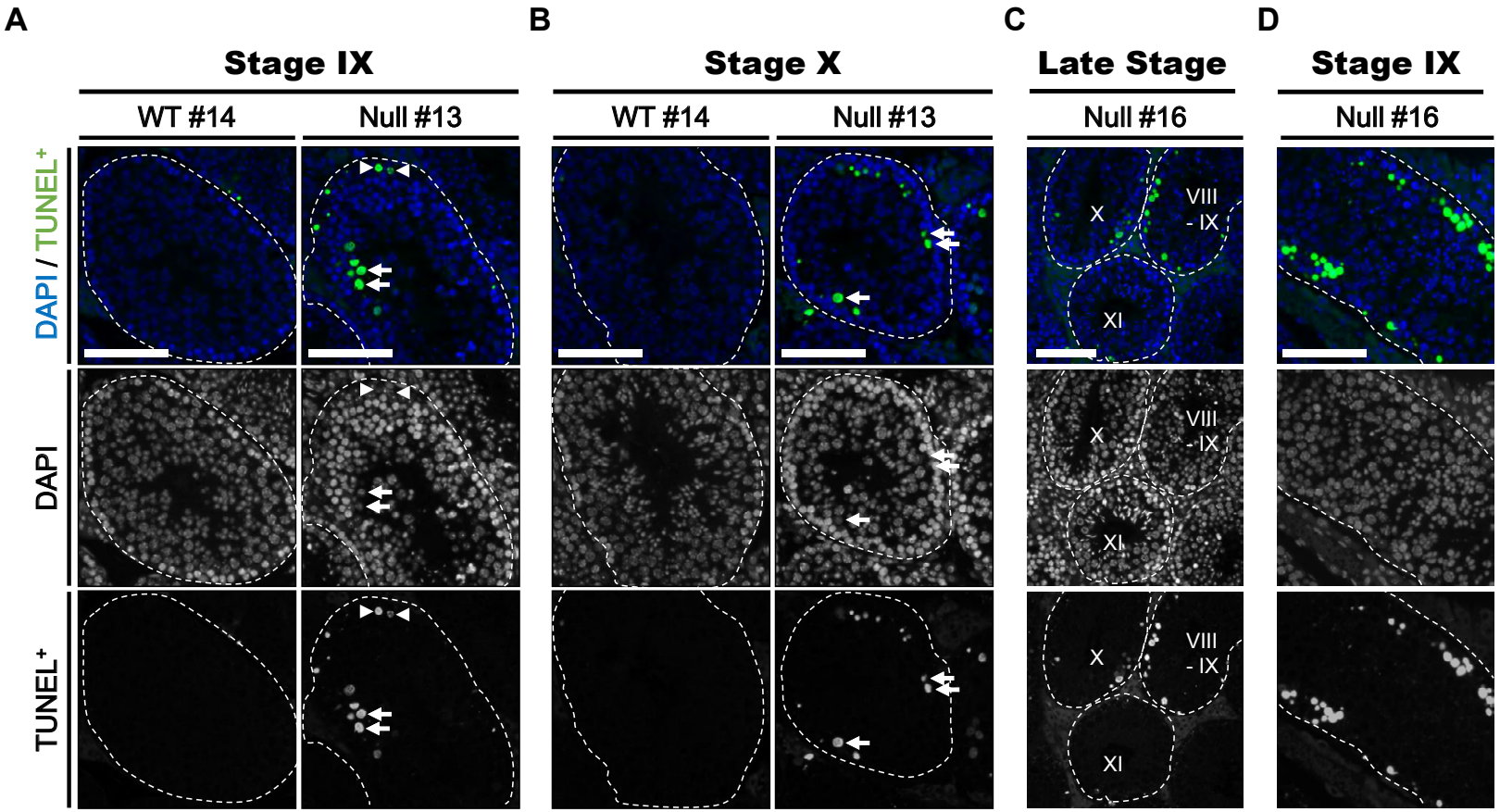

Yuen et al., Supplemental Figure 7

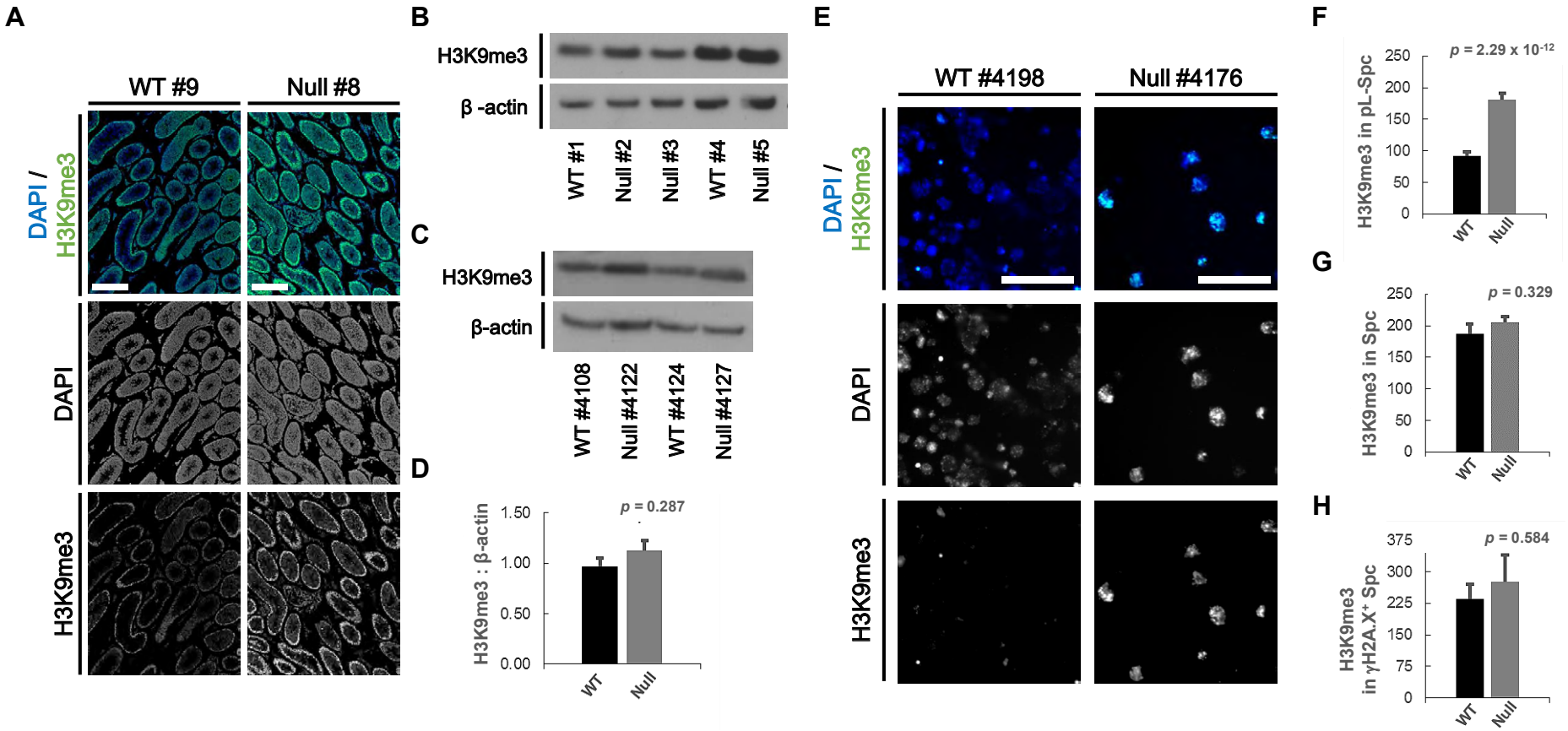

Yuen et al., Supplemental Figure 8

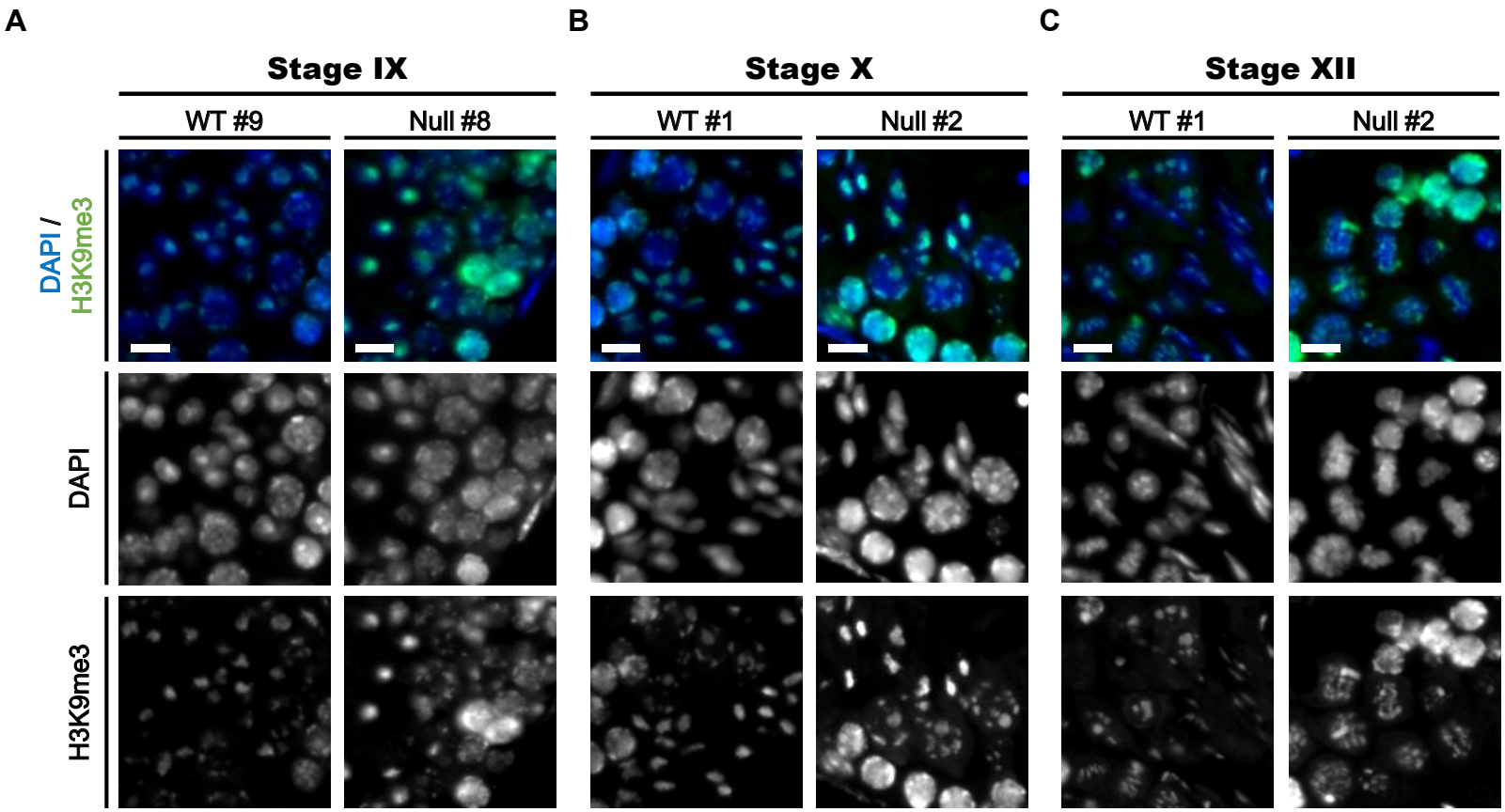

Yuen et al., Supplemental Figure 9

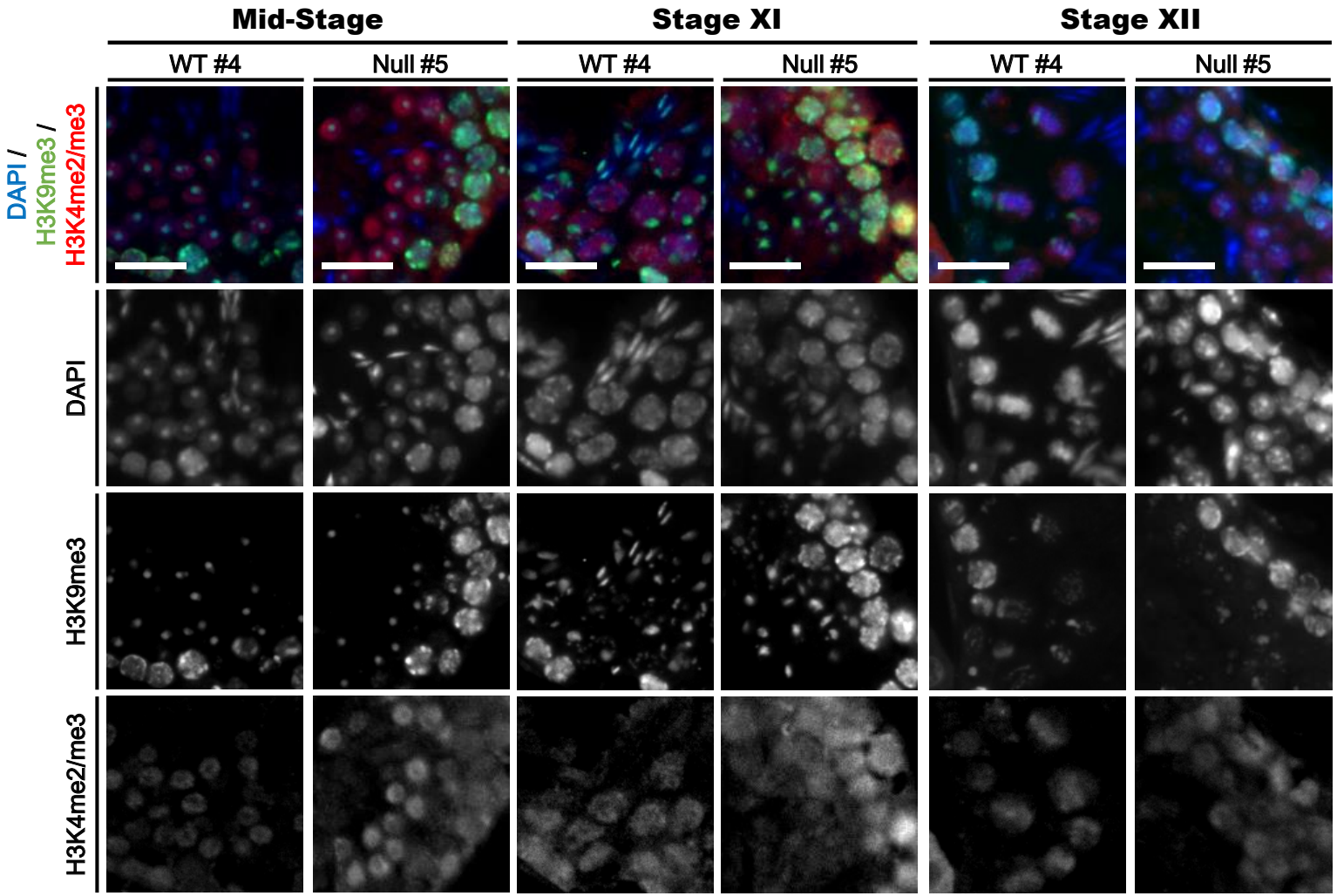

Yuen et al., Supplemental Figure 10

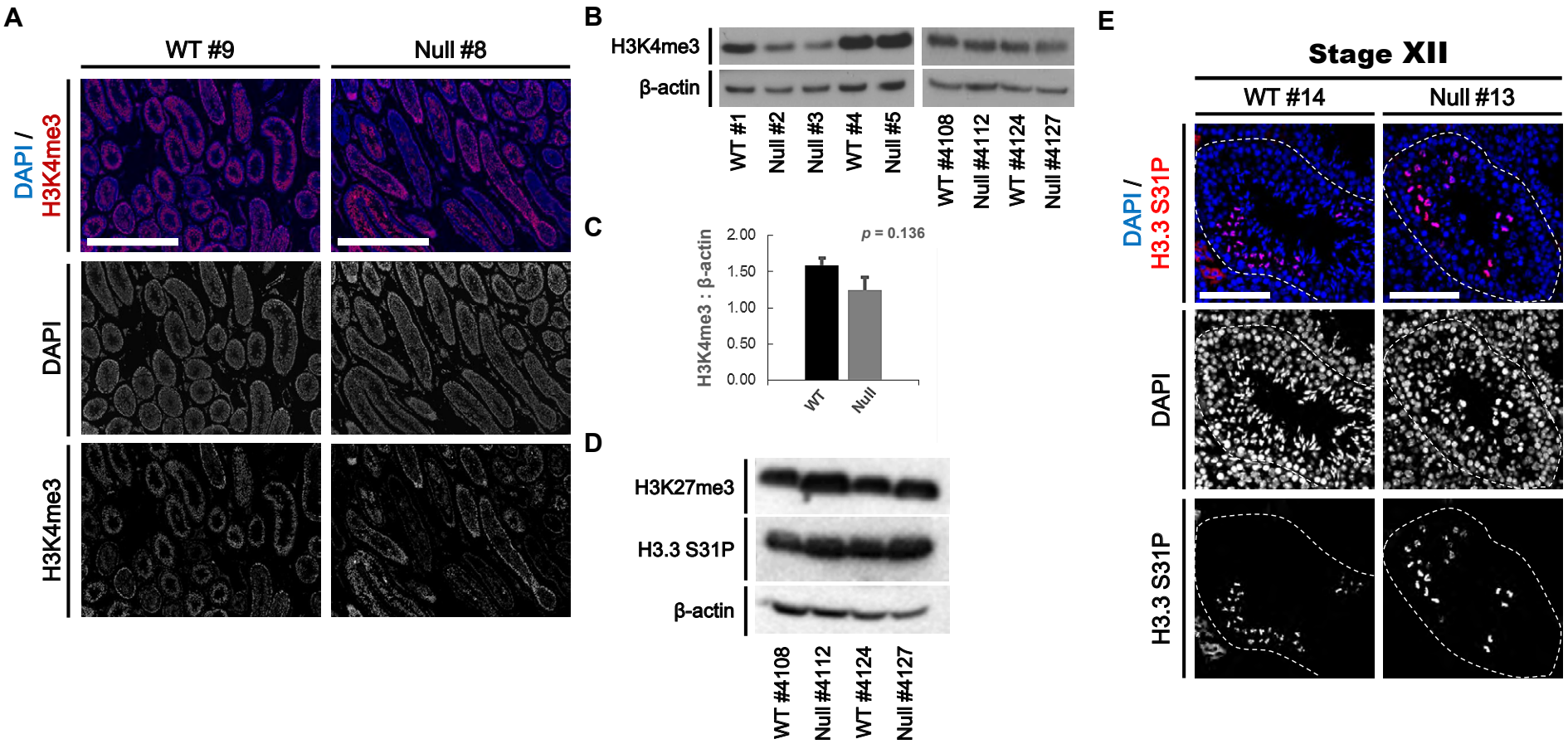

Yuen et al., Supplemental Figure 11

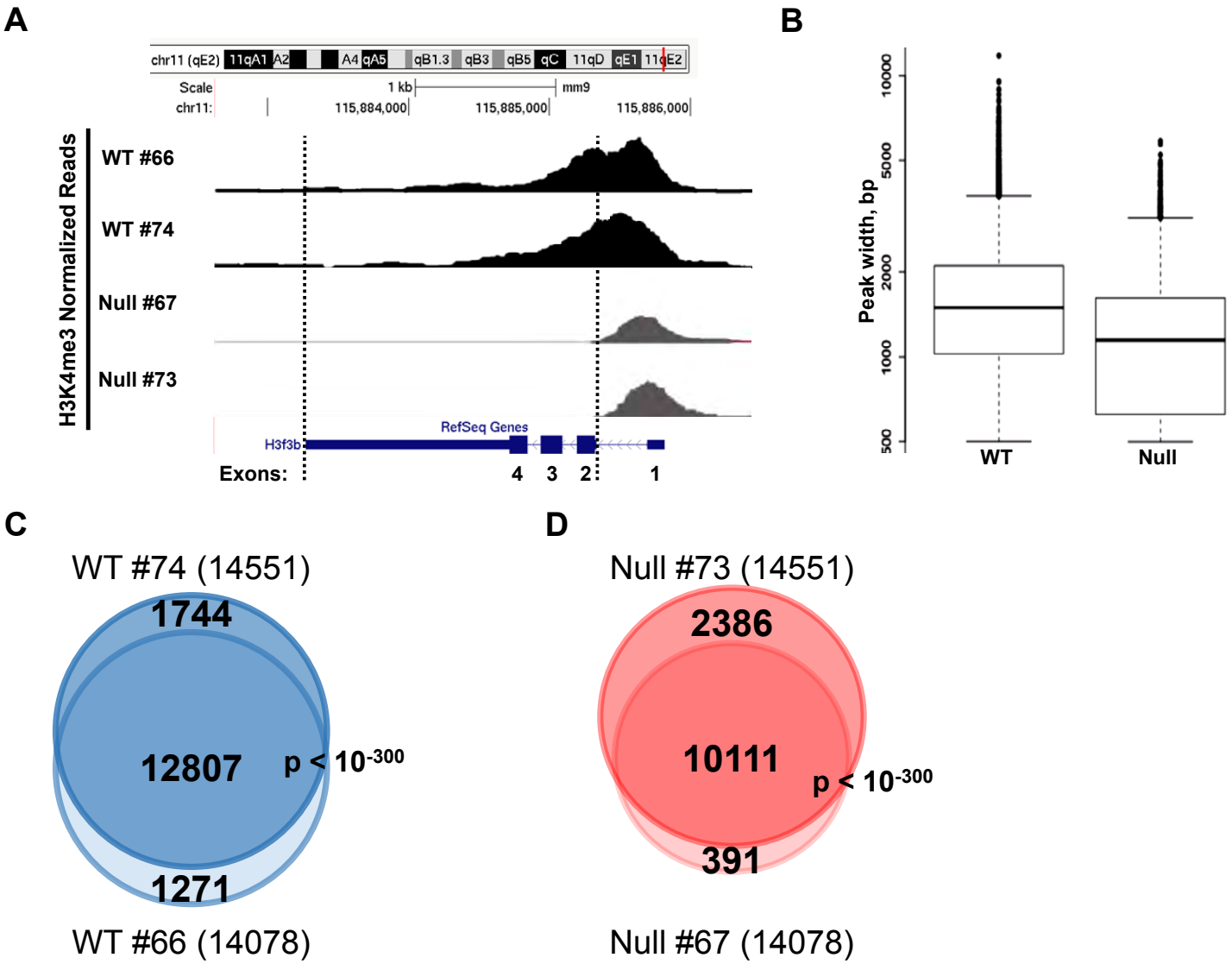

Yuen et al., Supplemental Figure 12

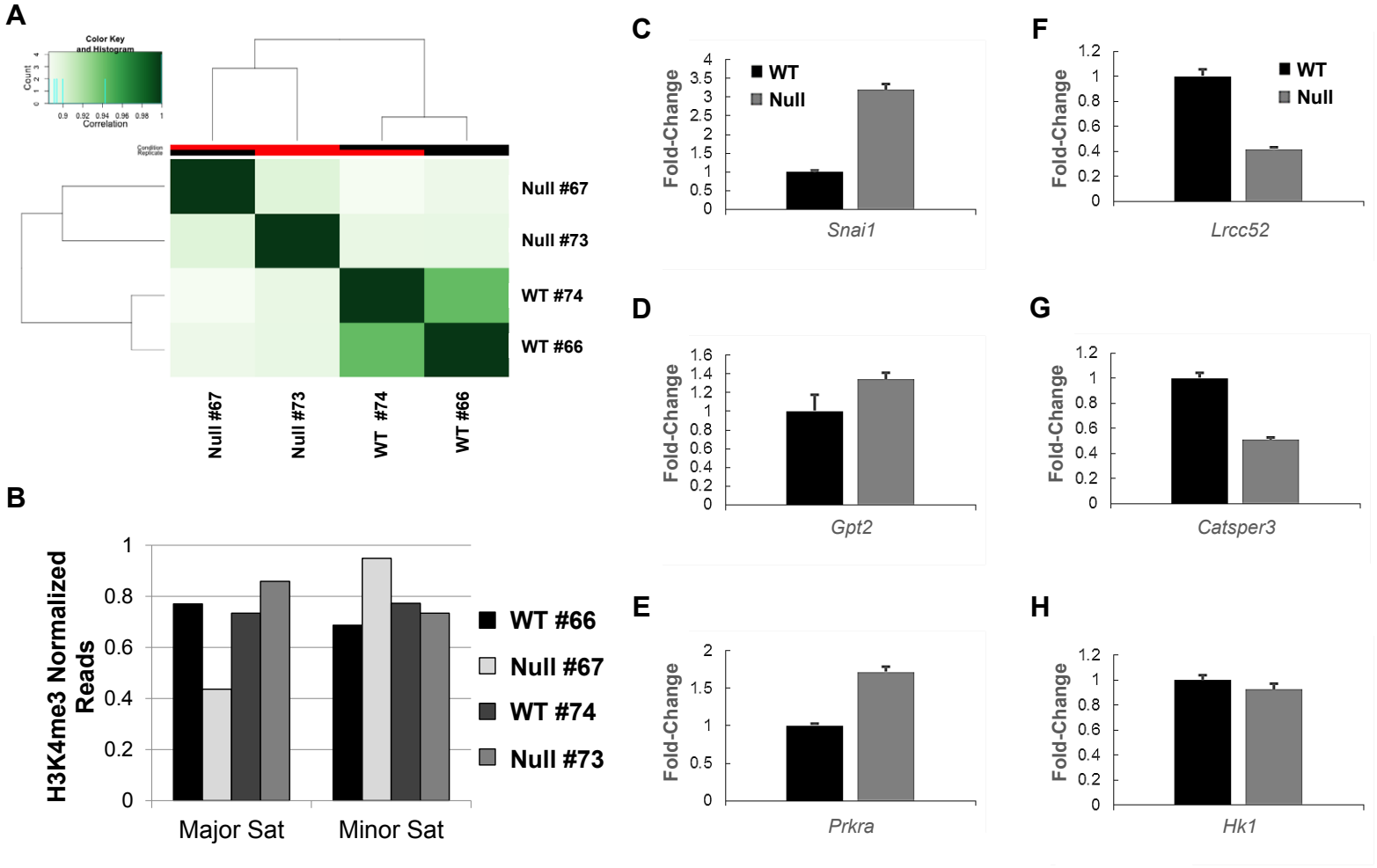

Yuen et al., Supplemental Figure 13

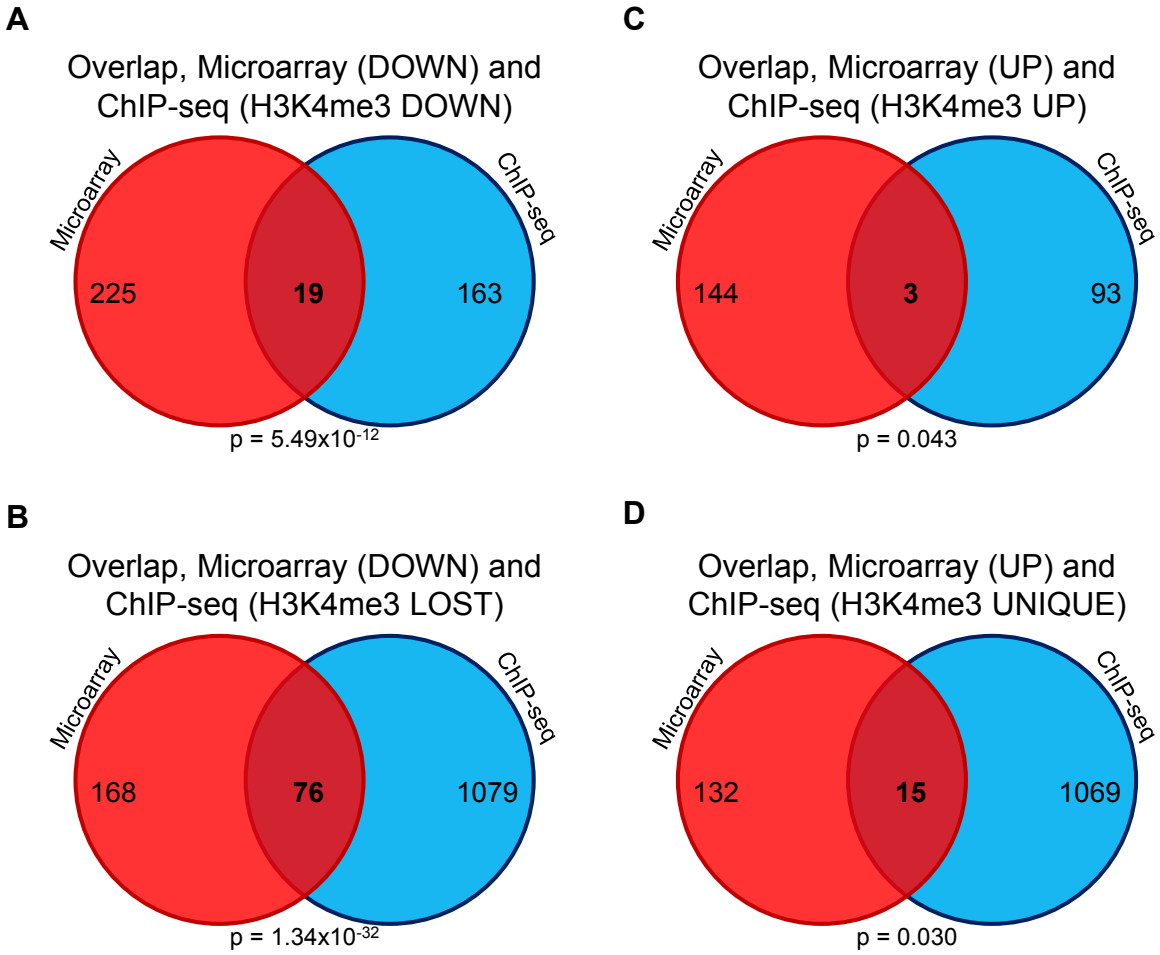

Yuen et al., Supplemental Figure 14

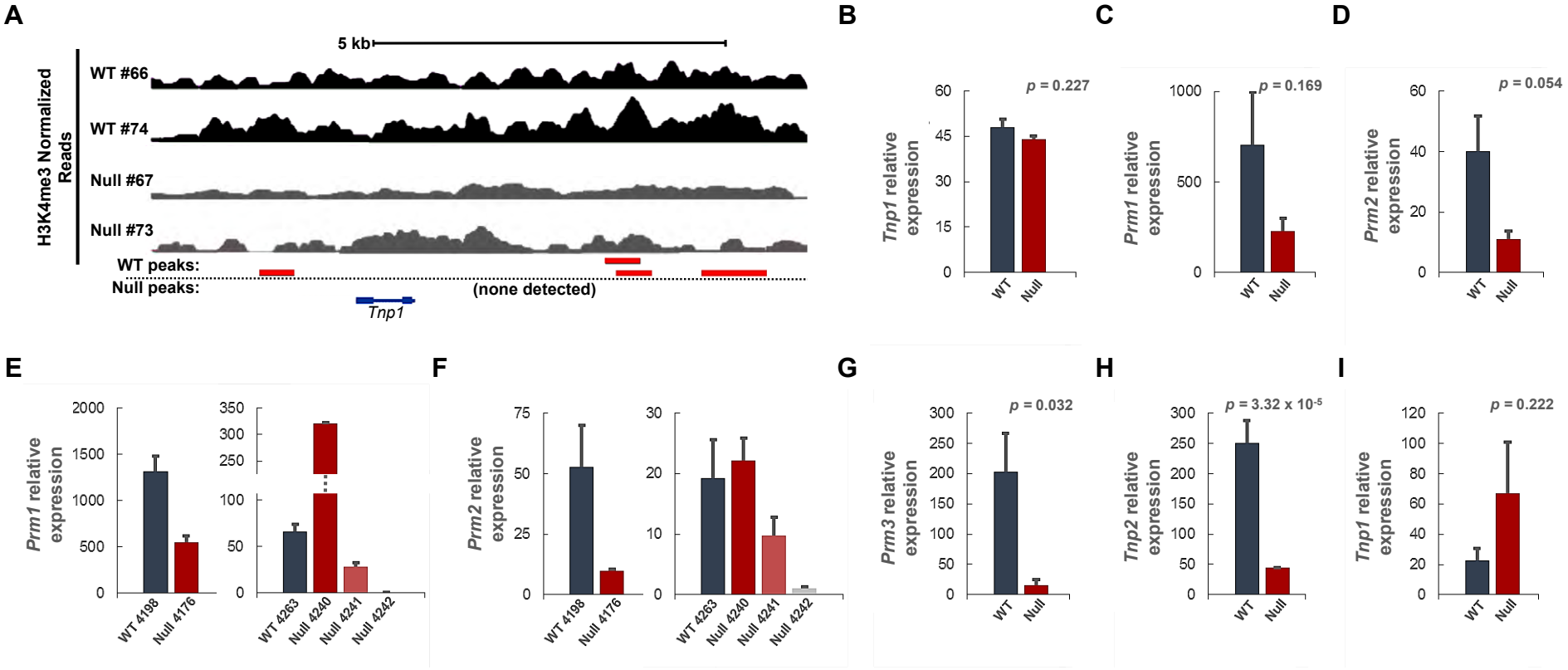

Yuen et al., Supplemental Figure 15

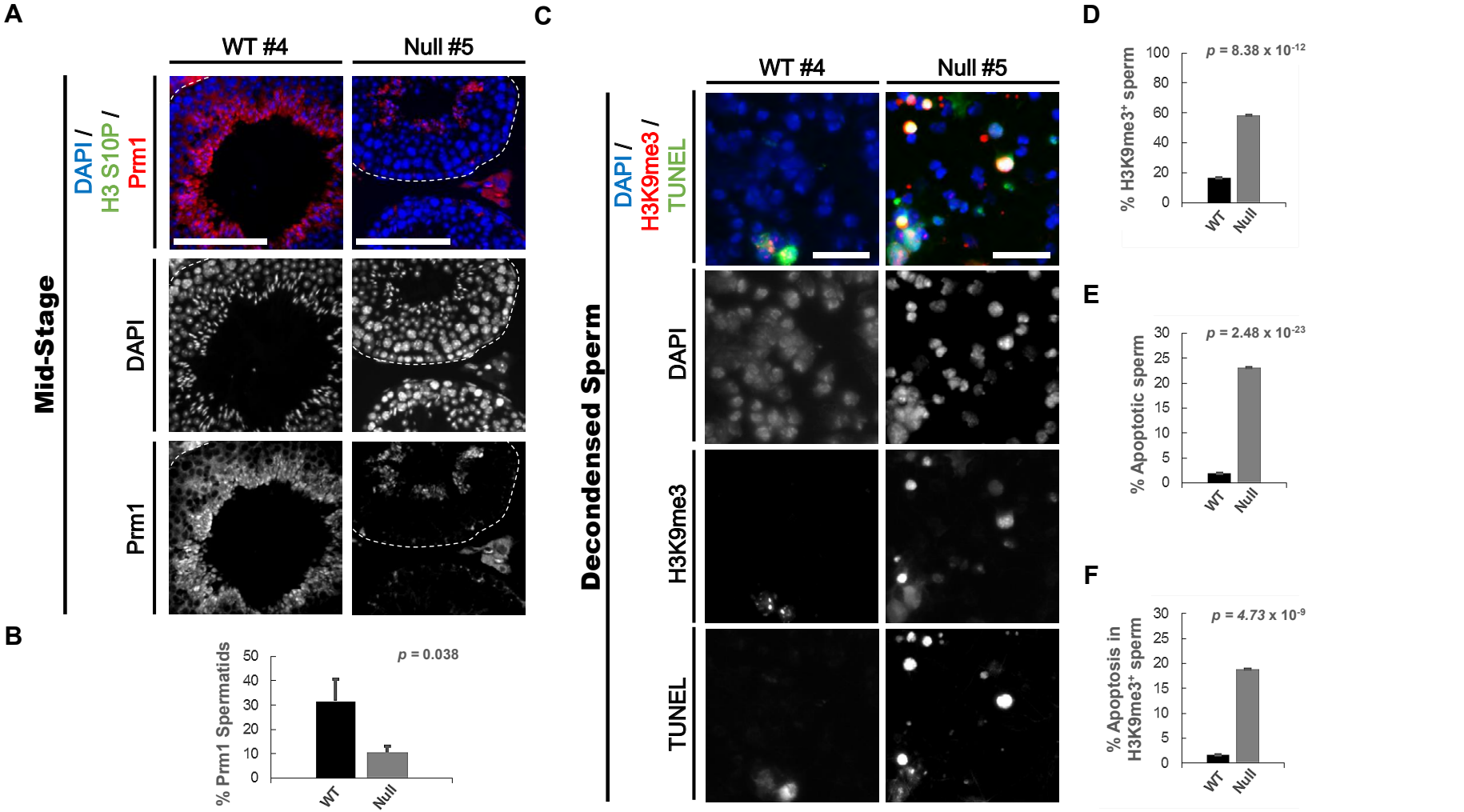

Yuen et al., Supplemental Figure 16

Movie 1.

Movie 2.

Download Table S1

Download Table S2

Download Table S3

Download Table S4

Download Table S5

Download Table S6

Download Table S7

Download Table S8